Antimicrob Agents Chemother. 2022 Jan 18;66(1):e0076721

Title: New insights into the mechanism of action of the cyclopalladated complex - **CP2** in *Leishmania*: Calcium Dysregulation, Mitochondrial Dysfunction and Cell Death

Angela M. A. Velásquez,[a,b] Paula J. Bartlett,[b] Irwin A. P. Linares,[c] Thais G. Passalacqua,[a] Daphne D. L. Teodoro,[a] Kely B. Imamura,[a] Stela Virgilio,[d] Luiz R. O. Tosi,[d] Aline de L. Leite,[e] Marilia A. R. Buzalaf,[e] Jecika M. Velasques,[f] Adelino V. G. Netto,[f] Andrew P. Thomas,[b] Marcia A. S. Graminha[a]#*

[a]São Paulo State University (Unesp), School of Pharmaceutical Sciences, Araraquara, São Paulo, Brazil.

[b]Department of Pharmacology, Physiology and Neuroscience, New Jersey Medical School, Rutgers, The State University of New Jersey, Newark, NJ, USA.

[c] Department of Chemistry, São Carlos Institute of Chemistry – IQSC, University of São Paulo (USP), São Carlos-SP, Brazil

[d]Department of Cellular and Molecular Biology, and Pathogenic Bioagents, Ribeirão Preto Medical School, University of São Paulo (USP), University of São Paulo, Ribeirão Preto-SP, Brazil

[e]Laboratory of Biochemistry, Department of Biological Sciences, Bauru School of Dentistry, University of São Paulo (USP), Bauru-SP, Brazil

[f]São Paulo State University (Unesp), Institute of Chemistry, Araraquara, São Paulo, Brazil.

Running Title: The mechanism of action of **CP2** in *Leishmania*

#Address correspondence to Marcia A. S. Graminha, marcia.graminha@unesp.br

*Present address: Departamento de Análises Clínicas – UNESP, Rodovia Araraquara-Jaú Km 01 s/n, Campus Ville, Araraquara, SP, Brazil.

ABSTRACT

The current treatment of leishmaniasis is based on few drugs that present several drawbacks such as high toxicity, difficult administration route, and low efficacy. These disadvantages raise the necessity to develop novel antileishmanial compounds allied to a comprehensive understanding of their mechanisms of action. Here, we elucidate the probably mechanism of action of the antileishmanial binuclear cyclopalladated complex $[Pd(dmba)(\mu\text{-}N_3)]_2$ (**CP2**) in *Leishmania amazonensis*. **CP2** causes oxidative stress in the parasite resulting in disruption of mitochondrial Ca^{2+} homeostasis, cell cycle arrest at S-phase, increasing the ROS production and overexpression of stress-related and cell detoxification proteins, collapsing the *Leishmania* mitochondrial membrane potential and promotes apoptotic-like features in promastigotes leading to necrosis or directs programmed cell death (PCD)-committed cells toward necrotic-like destruction. Moreover, **CP2** is able to reduce the parasite load in both liver and spleen in *Leishmania* infantum-infected hamsters when treated for 15 days with 1.5 mg/Kg/day **CP2**, expanding its potential application in addition to the already known effectiveness on cutaneous leishmaniasis for the treatment of visceral leishmaniasis, showing the broad spectrum of action of this cyclopalladated complex. The data herein presented bring new insights into the **CP2** molecular mechanisms of action, assisting to promote its rational modification to improve both safety and efficacy.

Keywords: Binuclear cyclopalladated complex, cutaneous leishmaniasis, leishmanicidal activity, necrotic death in *Leishmania*, calcium homeostasis, mitochondria.

INTRODUCTION

Leishmaniasis is a neglected parasitic disease caused by at least 20 species of the kinetoplastid genus *Leishmania* (1, 2) and is endemic in 98 countries (3). Cutaneous leishmaniasis (CL) is the most common clinical manifestation, while visceral leishmaniasis (VL) is a very severe systemic manifestation that can be fatal if left untreated (1, 2, 4). Causative CL species in the old-world are *L. tropica, L. major*, and *L. aethiopica*; also *L. infantum* and *L. donovani*. In the Americas (New-world) the species involved in CL are *L. mexicana* species complex (especially *L. mexicana, L. amazonensis,* and *L. venezuelensis*) and Viannia subgenus (most notably *L. (V.) braziliensis, L. (V.) panamensis, L. (V.) guyanensis,* and *L. (V.) peruviana*); also *L. major*-like organisms and *L. chagasi*. For VL, the principal causative species of disease are *L. donovani* species complex (ie, *L. donovani* and *L. infantum* in old-world, and *L. chagasi* in new-world) (5–7).

Available treatments for leishmaniasis have several limitations associated with high toxicity, difficult administration route, and low efficacy in endemic areas due to the emergence of resistant strains (4, 8–10). The adverse effects are mainly evident in leishmaniasis–HIV coinfection (1, 3). The current drugs for VL include pentavalent antimonials, amphotericin B and its lipid formulations (AmBisome), paromomycin, miltefosine, and drug combinations, such as AmBisome/miltefosine, AmBisome/paromomycin, and miltefosine/paromomycin (2, 4, 11). For the CL, limited treatments are available (pentavalent antimonials, amphotericin B, and pentamidine) in comparison to VL, where these drugs are only recommended for the treatment of specific forms (2, 12). These challenges associated with few current pharmaceuticals highlight the urgent need to develop novel, safe, and effective leishmaniasis treatment drugs.

Thus, in order to contribute to new molecules that overcome the problems listed above, different strategies to identify new drugs against *Leishmania* spp. have been used (13–

18). Many primary screenings of different compound libraries (natural products or synthetic molecules) have identified and validated hits (15, 19, 28–32, 20–27). Metal complexes with known antitumor bioactivity have been tested to treat various neglected diseases; some of them have exhibited anti-trypanosomatid effects (21, 24, 36–43, 25, 26, 28–30, 33–35). Moreover, the insertion of metal centers in antiparasitic drug structures is a strategy to increase their pharmacological activity by affecting multiple targets simultaneously (26). Au^{III} and Pd^{II} cyclometallated compounds and oxorhenium(V) complexes that inhibit different cysteine proteases of *Trypanosoma cruzi* and *Leishmania* spp. was developed as reported by Fricker and colleagues (25). Other authors reported the *in vitro* and *in vivo* leishmanicidal and trypanocidal activity of some Pd^{II} complexes (29, 30, 46, 33, 35–38, 43–45). However, not all of these reports addressed the possible mechanism of action of these compounds. In general, studies involving Pd^{II} complexes reported that these compounds induce arrest of the cell cycle of parasites, generation of reactive oxygen species (ROS), interaction with DNA by electrostatic forces, irreversible inhibition of trypanothione reductase and cysteine protease, and inhibition of topoisomerase I (25, 30, 38, 43, 45, 46). The palladacycle compounds $[Pd_2Cl_2(C^2,N\text{-dmpa})_2(\mu\text{-dppe})]$ (DPPE 1.1) and $[Pd(C^2,N\text{-dmpa})(dppe)]Cl$ (DPPE 1.2), where dmpa = $S_{(-)}$-*N,N*-dimethyl-1-phenethylamine, dppe = 1,2-Bis(diphenylphosphino)ethane, reduced the parasite load *L. amazonensis* infected mice and reported cathepsin B and cysteine protease as their targets. However, cell death mechanism induced by DPPE 1.1 and DPPE 1.2 has not been investigated (35–37). Other studies on DPPE 1.1 have described the cascade of effects produced after parasite treatment, and that also displayed action against other organisms (33, 34, 47). DPPE 1.1 exerts in *T. cruzi* trypomastigotes an apoptosis-like death and causes mitochondrion disruption (33); in *Paracoccidioides lutzii* and *P. brasiliensis*, the complex induced remarkable chromatin condensation, DNA degradation,

superoxide anion production, metacaspase activity, and apoptosis- and autophagy-like mechanisms (34). In murine and cisplatin-resistant human tumor cells, DPPE 1.1 interacts with mitochondrial membrane thiol-groups and induces the intrinsic apoptotic pathway (47).

Previously, we demonstrated that the binuclear cyclopalladated complex [Pd(dmba)(μ-N_3)]$_2$ (**CP2**) delivers *in vivo* leishmanicidal activity in a *L. amazonensis*-infected mice as a CL model via inhibition of DNA topoisomerase 1B (30). In this study we identified the downstream effects of the *Leishmania* topoisomerase IB inhibition by **CP2**, and its probable mechanism of action against *L. amazonensis*. Here, we observed that **CP2** increased ROS, cytosolic Ca^{2+} levels, and collapsed the mitochondrial membrane potential, leading the parasite to promote necrosis or leading programmed cell death (PCD) committed cells toward necrotic-like destruction. In addition, **CP2** causes an alteration in the levels of translation, stress-response proteins, and ROS detoxification in *L. amazonensis*. Finally, we demonstrated that **CP2** not only has *in vivo* leishmanicidal activity on CL model but also displayed effective leishmanicidal activity against *L. infantum*-infected hamsters, a VL model, which demonstrates the widespread potential of this cyclopalladated complex.

RESULTS

CP2 displayed *in vitro* and *in vivo* antileishmanial activity against *L. infantum*

143 To evaluate the spectrum of action of **CP2** beyond the effects previously reported (30),
144 we analyzed the *in vitro* and *in vivo* efficacy of the compound using *L. infantum* as the
145 causative agent of visceral leishmaniasis. **CP2** displayed a high antileishmanial activity
146 and selectivity index (SI) against both the insect promastigote stage (IC_{50} = 4.0 µmol L^{-1},
147 SI = 1261) and the intracellular amastigote forms (IC_{50} = 4.7 µmol L^{-1}, SI = 107.6) as
148 reported in Table 1. The SI values were calculated used our previously reported values of
149 cytotoxicity of **CP2** against murine peritoneal macrophages (30).

150

151 **TABLE 1** Antileishmanial activity of **CP2** against *Leishmania infantum* (IC_{50}). Data are
152 the mean and standard deviation from three independent experiments. The results are
153 expressed in (µmol L^{-1}).

	L. infantum IC_{50} ± SD (SI)*	
Compound	**Promastigote**	**Amastigote**
CP2	4.0 ± 0.4 (126.1)	4.7 ± 0.1 (107.6)
AmpB	0.9 ± 0.1 (25.1)	2.9 ± 0.1 (7.7)

154 *The selectivity index (SI, indicated in parentheses) was calculated as the CC_{50}/IC_{50} of
155 **CP2**. $p < 0.05$ for all values.

156

157 *L. infantum*-infected Golden hamsters were used as a VL model. The animals were
158 treated for 15 days with **CP2** (0.75 or 1.5 mg/Kg/day) or AmpB (20 mg/Kg/day) and the
159 parasite load of both spleen and liver determined (Fig. 1). A dose of 1.5 mg/Kg/day of
160 **CP2** caused a ~50% reduction in the parasite load of both liver and spleen similar to
161 AmpB (at a dose thirteen-fold higher than **CP2**), without any alteration in biochemical

markers of liver and kidney function (Fig. S1 at http://hdl.handle.net/11449/214617), following previous work (30).

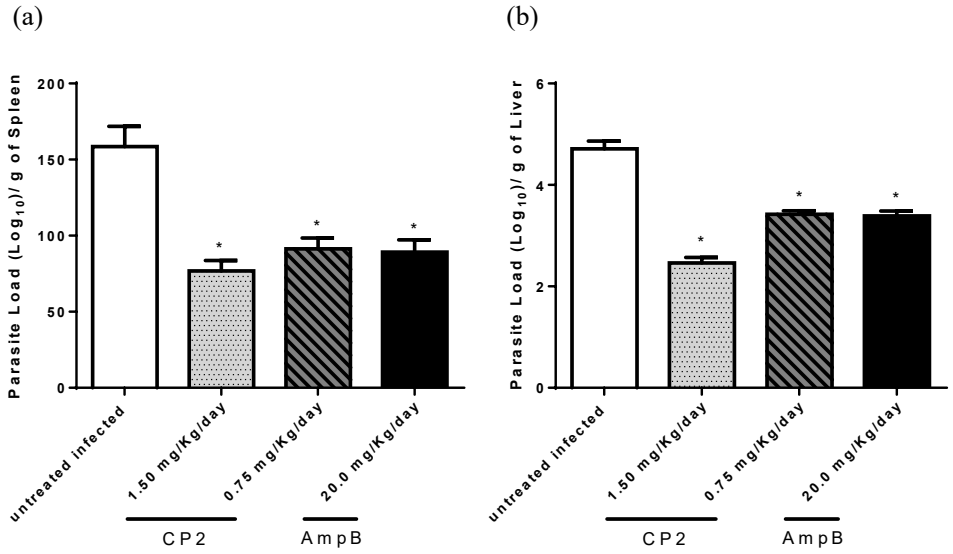

Fig. 1. Parasite load of *L. infantum*-infected hamsters treated with **CP2** or AmpB. Hamsters infected with *L. infantum* promastigotes in the stationary growth phase were treated with **CP2** or AmpB commencing 75 days post-infection for 15 days. The parasite load was determined by the limiting dilution method at the end of the treatment in (a) the spleen and (b) the liver. The data are expressed as mean ± SD.* Statistical significance of the difference relative to the untreated infected group ($p < 0.05$) was determined by ANOVA with Tukey's post-hoc test.

CP2 causes an alteration in the levels of stress-response proteins, protein translation and ROS detoxification in *Leishmania*

Two-dimensional SDS-PAGE comparative analysis was performed to identify differentially expressed proteins in the presence or absence of **CP2**. *L. amazonensis* promastigotes at logarithm growth phase were treated with 13.3 µmol L^{-1} of **CP2** for 72

h, concentration corresponding to the previously determined IC_{50} value (30). The protein extracts obtained were separated by two-dimensional SDS-PAGE in a pH ranging from 4 to 7 (Fig. S2 at http://hdl.handle.net/11449/214617).

Fifty two differentially expressed proteins identified through mass spectrometry analyses (Table S1 at http://hdl.handle.net/11449/214617) are related to chaperons/protein folding (48%), mitochondrial respiratory chain (17%), and ROS detoxification (14%), in addition to α- and β-tubulins. In order to minimize possible artifacts, the spots were selected after data filtration based on two factors: a *p*-value of less than 0.5 in a Student's t-test comparing protein samples obtained in the presence or absence of **CP2**, and expression differences higher than two-fold.

Among the overexpressed proteins, **CP2** increased the levels of putative chaperons by at least three fold, including HSP70, LMXM_28_2770 (nine-fold), two isoforms of putative calreticulin, LMXM_30_2600 (seven-fold – pI 4.14 and two-fold – pI 4.53), and protein disulfide-isomerase (PDI), LMXM_36_6940 (three-fold). For the group of redox proteins, trypanothione reductase, LMXM_05_0350, and the peroxidoxin tryparedoxin peroxidase, LMXM_23_0040, increased by six- and four-fold, respectively.

Some proteins related to parasites' mitochondria were found overexpressed in presence of **CP2** such as mitochondrial cytochrome c oxidase subunit IV, LMXM_12_0670, and ribonucleoprotein p18, LMXM_15_0275, while others, such as putative mitochondrial chaperone heat shock 70-related protein 1 (mHSP70-1), LMXM_29_2550, was not expressed in the cells treated with **CP2**.

In the functional category of protein synthesis, the putative translation elongation factor 1-beta, LMXM_33_0840, was eleven-fold higher relative to the control, while the elongation factor 1-alpha, LMXM_17_0080, the elongation factor 2, LMXM_36_0180, and the 60S acidic ribosomal protein P0, LMXM_27_1380, were only expressed in the

absence of **CP2**. The putative carboxypeptidase, LMXM_32_2540), in the category of amino acid metabolism, was incremented by two-fold. Additionally, RT-qPCR data also show a correspondence between transcriptional and protein levels for calreticulin, PDI, and tryparedoxin peroxidase (Fig. S3 at http://hdl.handle.net/11449/214617) induced by **CP2** (Fig. 2).

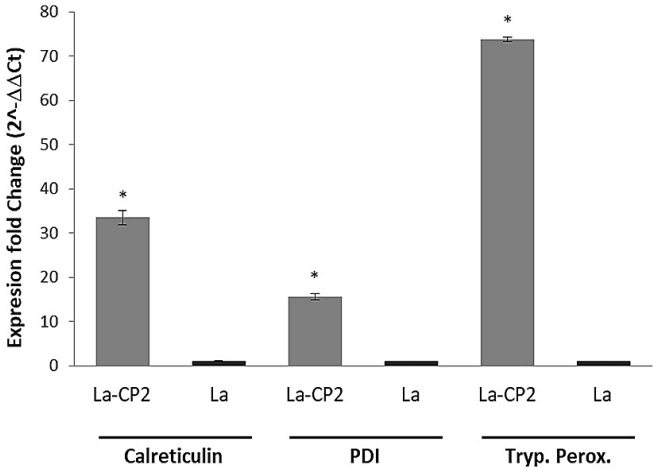

Fig. 2. Relative gene expression of calreticulin, PDI, and tryparedoxin peroxidase of *Leishmania amazonensis* promastigotes after 72 h of exposure to **CP2**. The relative gene expression determined by RT-qPCR was calculated using the $2^{-\Delta\Delta Ct}$ method, using kDNA mRNA expression as a reference and the *L. amazonensis* (La) in the absence of **CP2** as the calibrator (see the supplemental material at http://hdl.handle.net/11449/214617). The data were expressed as average ± SD.*: Statistical significance of the difference relative to La in the absence of **CP2**, control ($p < 0.001$) was determined by ANOVA with Tukey's post-hoc test. La-CP2 is the *L. amazonensis* treated with 13.3 µmol L^{-1} **CP2.**

220 **CP2 arrests cell cycle progression at S-phase in *Leishmania***

221 Previously, we demonstrated that **CP2** inhibited the cleavage step of DNA topoisomerase
222 1B of *Leishmania* (30), leading to the accumulation of DNA damage and arrest in the cell
223 cycle progression. To investigate the effect of **CP2** on cell cycle progression, hydroxyurea
224 (HU) synchronized *L. amazonensis* promastigotes were treated with **CP2** or **CP2** plus the
225 ROS inhibitor N-acetyl L-cysteine (NAC), and the progression of the cell cycle was
226 followed by determining the parasite DNA content by flow cytometry (Fig. 3).

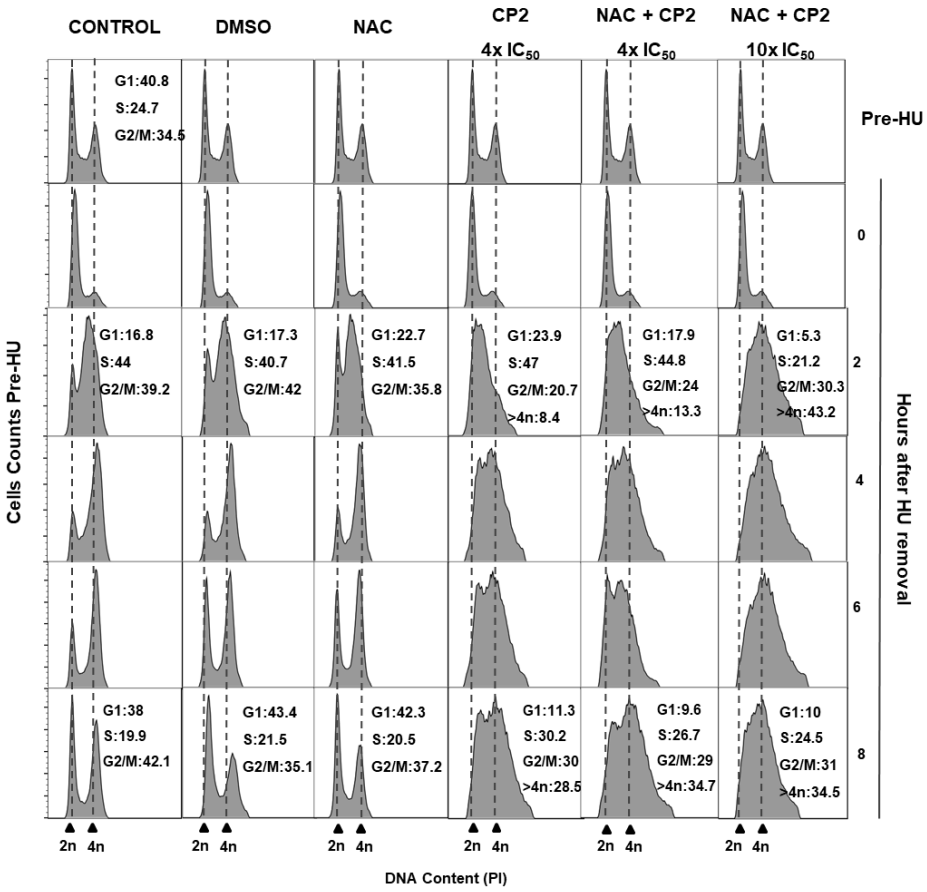

227

228 **Fig. 3. CP2** effect on the cell cycle of *Leishmania amazonensis*. Promastigotes in the
229 mid-log growth phase were synchronized by adding 5 mmol L^{-1} HU for eight hours and
230 then transferred to an HU-free medium containing 0.03% DMSO (control). The parasites

were treated with **CP2** (4 x IC_{50}: 53.2 µmol L^{-1}), 20 µmol L^{-1} NAC or **CP2** (4 x IC_{50}: 53.2 µmol L^{-1} or 10x IC_{50}: 133 µmol L^{-1}) plus 20 µmol L^{-1} NAC. Cells were collected at 0, 2, 4, 6, and 8 h, and the DNA content was measured by flow cytometry. Each histogram represents the data of 50,000 events; 2n and 4n indicate non-replicated and replicated DNA, respectively. The percentage of cells in G1, S, and G2/M phases is indicated for cells before treatment with HU (Pre-HU) and at 2 h and 8 h after the removal of HU. HU, hydroxyurea; NAC, N-acetyl-L-cysteine. ($p < 0.01$).

The data obtained demonstrate that **CP2** induced the accumulation of a higher proportion of cells in the S-phase, indicating an arrest of the cell cycle at this phase after **CP2** treatment at 53.2 µmol L^{-1}. Notably, this effect is not abolished by the addition of NAC. Moreover, promastigotes in the presence of 133 µmol L^{-1} **CP2** (10 x IC_{50}) increased the proportion of cells with 4n DNA content, indicating that the effect of **CP2** on the parasite cell cycle progression occurred independently of ROS.

CP2 increases ROS levels in *Leishmania*

Promastigotes were exposed for 60 min to different concentrations of **CP2** to determine its ability to increase cellular ROS levels at every 5 min. **CP2** increased ROS production in a dose-dependent manner (Fig. 4). This finding correlates with the proteomic data that showed overexpression of trypanothione reductase, peroxiredoxin, and tryparedoxin peroxidase, enzymes involved in the trypanothione-mediated hydroperoxide metabolism for detoxification of endogenous or exogenous oxidative agents (48).

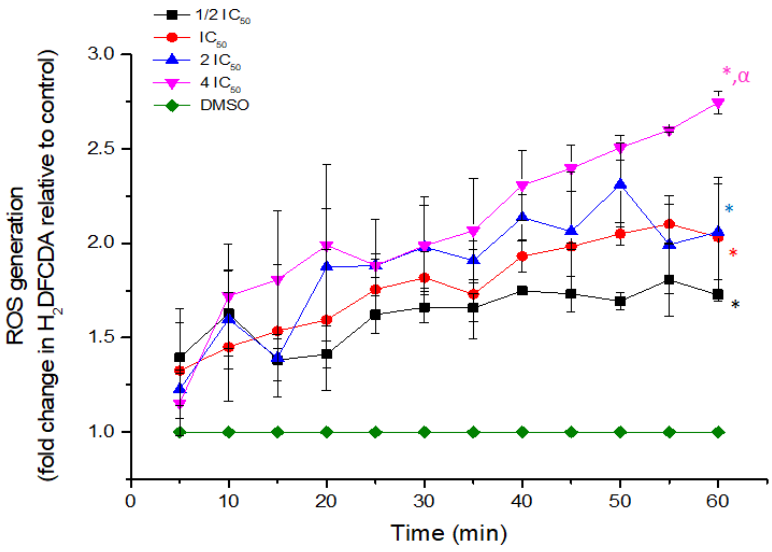

253 **Fig. 4. CP2**-dependent ROS generation in *L. amazonensis*. Promastigote forms of *L.*
254 *amazonensis* were treated with **CP2** (½ x IC_{50}: 6.7 µmol L^{-1}; IC_{50}: 13.3 µmol L^{-1}; 2 x IC_{50}:
255 26.6 µmol L^{-1} and 4 x IC_{50}: 53.2 µmol L^{-1}) for 60 min. ROS generation was measured
256 spectrofluorimetrically using the probe H_2DFCDA. The parasites were treated with 0.1%
257 DMSO as a control. Data are mean ± SD of three independent experiments. *: statistically
258 significant difference relative to DMSO control ($p < 0.001$); α: statistically significant
259 difference relative to parasites treated with ½ x IC_{50} of **CP2** ($p < 0.01$). Statistical
260 significance was determined by ANOVA with Student-Newman-Keuls multiple
261 comparisons test.

262

263 **CP2 disrupts Ca^{2+} homeostasis in *Leishmania* in a dose-dependent manner**

264 Considering that oxidative stress is often associated with a rise in intracellular Ca^{2+}
265 concentration ($[Ca^{2+}]_i$) (49–52), we determined the effect of **CP2** on $[Ca^{2+}]_i$ in single-
266 promastigote cells by live-cell fluorescence imaging using the ratiometric Ca^{2+} indicator
267 Fura-2/AM (Fig. 5). After **CP2** addition, increases in $[Ca^{2+}]_i$ were observed in the

majority of cells after a delay of 5-10 min. The subsequent addition of the Ca^{2+} ionophore ionomycin increased $[Ca^{2+}]_i$ to maximum, and this occurred with no delay. The presence of an ionomycin response and maintenance of the Fura-2 dye load of the cells was used to validate that the cells remained viable during the experiment. The $[Ca^{2+}]_i$ responses to **CP2** varied in magnitude, with an increase to near-maximal $[Ca^{2+}]_i$ levels (relative to the ionomycin response) in some promastigotes (Fig. 5a). In contrast, others exhibited small peaks and only partial increases in $[Ca^{2+}]_i$ (Fig. 5b). When the responses were averaged from all parasites in the imaging field, the profile $[Ca^{2+}]_i$ showed a progressive increase during the incubation period (Fig. 5c). Additionally, the percentage of parasites that exhibited changes in $[Ca^{2+}]_i$ during the incubation period with **CP2** increased in a dose-dependent manner (Fig. 5d). In the presence of 3.8 µmol $L^{-1,}$ an increase in $[Ca^{2+}]_i$ was detected in 20% of cells during the 25-30 min time-course of the experiment, whereas in the presence of 7.5 µmol L^{-1} and 15 µmol L^{-1} responses were detected in 60% and 98% of cells, respectively. Following the large $[Ca^{2+}]_i$ increase during continuing incubation with high doses of **CP2**, some cells showed a loss of the total Fura-2 signal, which was taken as an indicator of cell death (Fig. S4 at http://hdl.handle.net/11449/214617). Thus, the increase in Ca^{2+} levels appears to presage cell death in response to **CP2** (Fig. 5c).

Removal of extracellular Ca^{2+} did not affect the percentage of promastigotes of *L. mexicana* exposed to **CP2**, in which increases in $[Ca^{2+}]_i$ were observed (Fig. 6a, 6b). These data show that **CP2**-induced $[Ca^{2+}]_i$ responses are observed in the absence of extracellular Ca^{2+}, indicating that the observed $[Ca^{2+}]_i$ increase is caused by Ca^{2+} release from an intracellular Ca^{2+} store, such as the endoplasmic reticulum (ER), acidic compartments or mitochondria. Of note, an increase in dead cells after **CP2** addition was also still observed in the absence of extracellular Ca^{2+} (Fig. 6c).

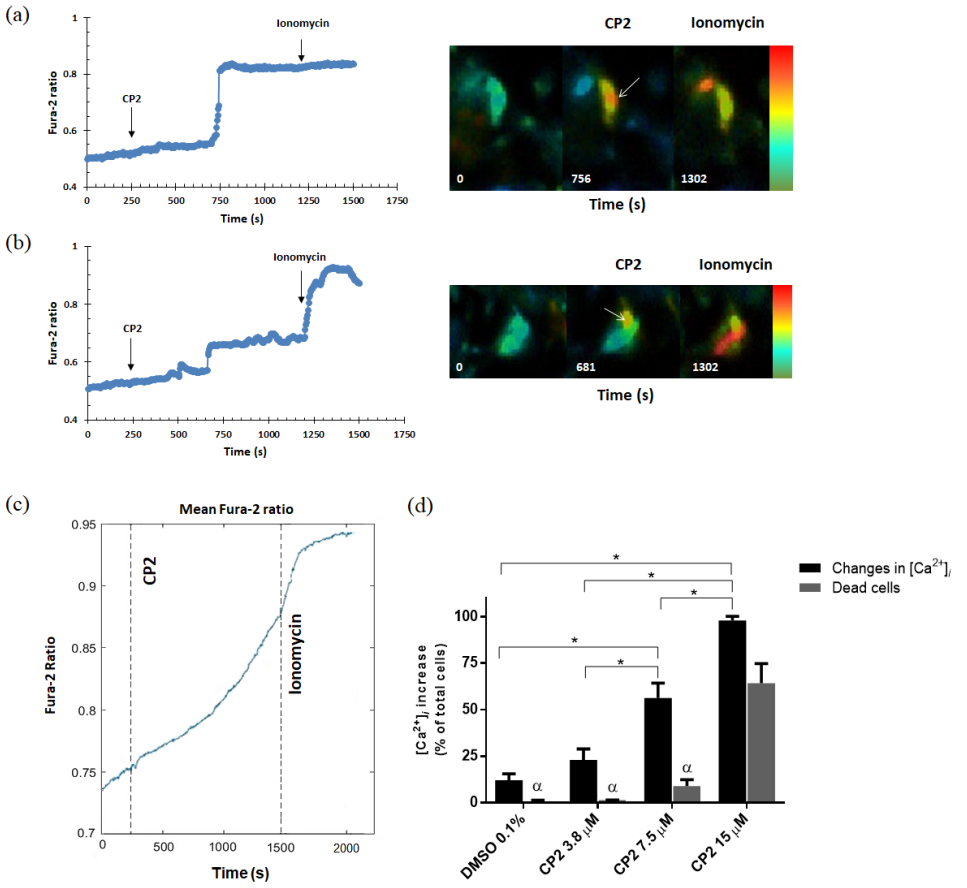

Fig. 5. Effect of **CP2** on the $[Ca^{2+}]_i$ of *Leishmania mexicana* promastigotes. The parasites were cultivated until the mid-log growth phase and then loaded with 5 µmol L^{-1} Fura-2/AM in a loading buffer containing 1.3 mmol L^{-1} of $CaCl_2$. Changes in $[Ca^{2+}]_i$ were measured with Fura-2 excitation at 340/380 nm and emission at > 510 nm and are plotted as the 340/380 ratio (Fura-2 ratio). Representative single-cell traces of large (a) and small (b) $[Ca^{2+}]_i$ changes in response to 7.5 µmol L^{-1} **CP2** treatment of promastigotes are shown. Ionomycin (10 µmol L^{-1}) was added at the end of each experiment to determine the maximal $[Ca^{2+}]_i$ response for each cell. The right panel shows pseudocolor images demonstrating the increase in fluorescence ratio related to an increase in $[Ca^{2+}]_i$ from blue (lowest ratio) to red (highest ratio) in the absence and presence of

drugs. (c) Averaged trace for 100 cells in the imaging field. (d) Mean percentage of parasites with a change in $[Ca^{2+}]_i$ in the presence of 3.8, 7.5, or 15 µmol L^{-1} **CP2**, 0.1 % DMSO was used as a control. Cell death counts reflect cells that showed total loss of Fura-2 by the end of the imaging experiment. Summary data are mean ± SD of three independent experiments. α:statistically significant difference relative to dead cells in the presence of 15 µmol L^{-1} **CP2**, and *: statistically significant difference between groups ($p < 0.001$) was determined by Two-way ANOVA followed by Tukey's multiple comparisons test.

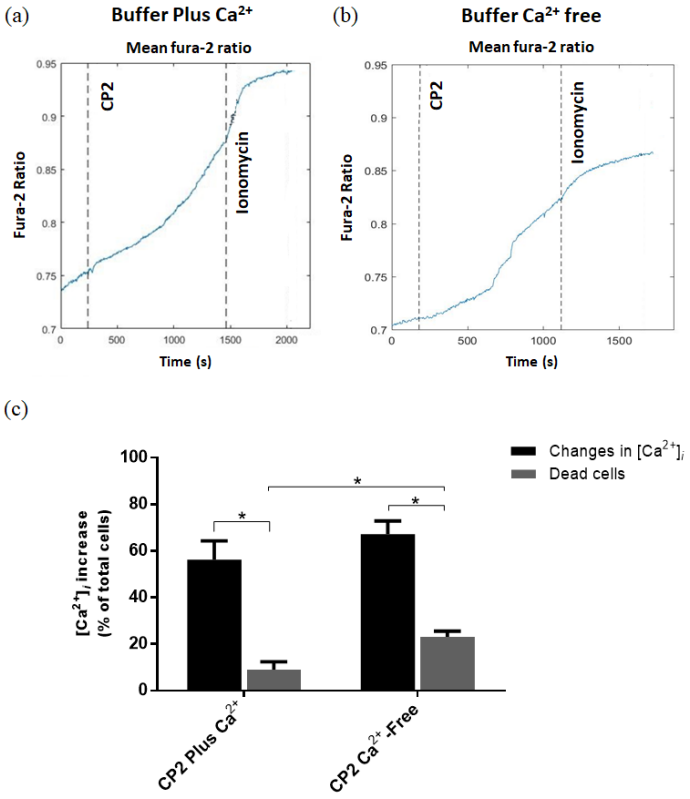

Fig. 6. Removal of extracellular Ca^{2+} does not perturb **CP2**-induced $[Ca^{2+}]_i$ responses in *Leishmania mexicana*. A representative experiment of promastigotes cultivated until the

mid-log growth phase and then loaded with Fura-2/AM in a loading buffer with (a) or without (b) 1.3 mmol L^{-1} of $CaCl_2$ and treated with 7.5 µmol L^{-1} **CP2** followed by 10 µmol L^{-1} ionomycin. Traces averaged from 100 individual parasites. (c) Mean of the percentage of parasites with an increase in $[Ca^{2+}]_i$ and the percentage of dead cells in the presence or absence of extracellular Ca^{2+} after **CP2** addition. Summary data are mean ± SD of three independent experiments. *: statistically significant difference between groups ($p < 0.001$) was determined by Two-way ANOVA followed by Tukey's multiple comparisons test.

The metal chelator TPEN does not suppress the CP2-dependent $[Ca^{2+}]_i$ response.

Since **CP2** is a complex of Pd^{2+}, and heavy metals can affect Ca^{2+} channels and pumps, we tested the effect of TPEN (N,N,N′,N′-Tetrakis (2-pyridylmethyl) ethylenediamine), a permeable cell and highly selective heavy metal chelating agent with low affinity for Mg^{2+} and Ca^{2+} (53, 54). *L. mexicana* promastigotes were exposed to 10 µmol L^{-1} TPEN followed by **CP2** addition (3.8 and 7.5 µmol L^{-1}) (Fig. 7). It was observed that TPEN does not inhibit the ability of **CP2** to mobilize intracellular Ca^{2+} (Fig. 7a, 7b). **CP2** (7.5 µmol L^{-1}) induced $[Ca^{2+}]_i$ responses was observed in ~60% of cells in the presence or absence of TPEN (Fig. 7c). Heavy metals have been shown to alter the fluorescent properties of Ca^{2+} indicator dyes (53). The addition of **CP2** does not alter the fluorescence of Fura-2 in *Leishmania,* and TPEN does not perturb the Ca^{2+} response to this agent indicates that Pd^{2+} is coordinated to *N,N*-dimethylbenzylamine (dmba), and azide (N_3^-) in the active species of **CP2**, which contributes to its effect on $[Ca^{2+}]_i$ mobilization. Notably, the dmba by itself did not exhibit leishmanicidal activity, as previously demonstrated (29). Nevertheless, it cannot be ruled out that **CP2** can participate in competing ligand

339 exchange reactions with other molecules or bridge splitting reactions during the
340 experiments, affording new species, which may be responsible for the observed activity.

341

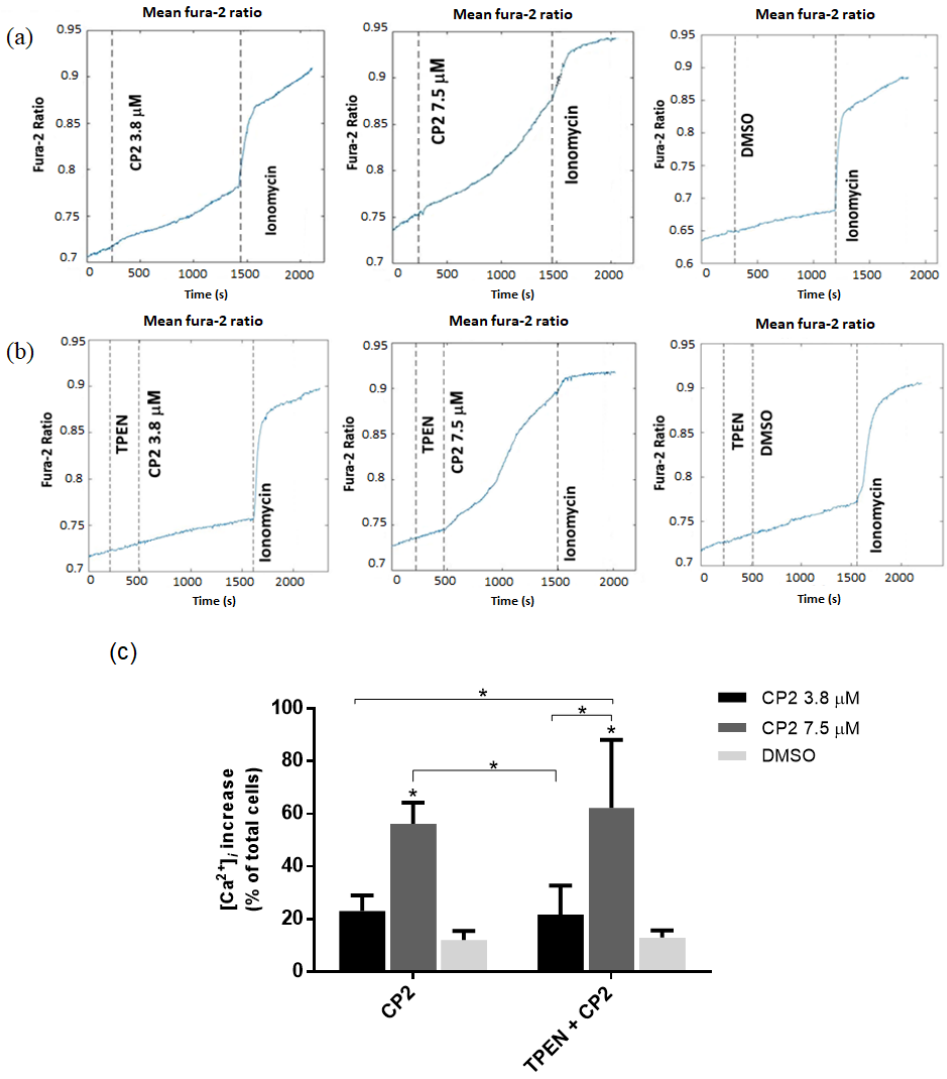

342

343 **Fig. 7**. Effect of **CP2** on the *L. mexicana* $[Ca^{2+}]_i$ in the presence of TPEN, a heavy metal
344 chelating agent. (a) Representative experiment of promastigotes treated with 3.8 or 7.5
345 µmol L^{-1} **CP2** followed by 10 µmol L^{-1} ionomycin and (b) promastigotes treated with 10
346 µmol L^{-1} TPEN plus 3.8 or 7.5 µmol L^{-1} **CP2**, followed by 10 µmol L^{-1} ionomycin. Each

trace is the average from at least 100 individual parasites. (c) Summary data of the percent of cells with increased $[Ca^{2+}]_i$, 0.1 % DMSO was used as a control. Data are mean ± SD of three independent experiments. *: statistically significant difference relative to DMSO control ($p < 0.001$) was determined by Two-way ANOVA followed by Tukey's multiple comparisons test.

CP2 induces Ca^{2+} release from mitochondria but not ER or acidic Ca^{2+} pools in *Leishmania*

Fura-2/AM-loaded promastigotes in the presence of extracellular Ca^{2+} were exposed to nigericin (55) or cyclopiazonic acid (CPA) (56), followed by the addition of **CP2** in order to determine the Ca^{2+} store targeted by **CP2**. The addition of nigericin, which releases Ca^{2+} from acidic compartments such as the acidocalcisome and acidic vesicles, resulted in an elevation of $[Ca^{2+}]_i$ in ~60% of the parasites. Nevertheless, an increase in $[Ca^{2+}]_i$ was still observed after adding **CP2** to nigericin-treated cells in 90% of the cells. Also, in cells, that response to nigericin, an additional increase in response **CP2** was observed in ~77% (Fig. 8a and 8b). Thus, **CP2** does not act by mobilizing Ca^{2+} from acidic pools in *Leishmania*.

CPA, a specific inhibitor of the sarco-endoplasmic reticulum Ca^{2+}-ATPase (SERCA) (56), was used to investigate whether **CP2** releases Ca^{2+} from the ER. Ca^{2+} responses in Fura-2 loaded parasites were observed after the addition of both CPA and **CP2,** suggesting that the release of Ca^{2+} caused by these two drugs is independent (Fig. 9a). Almost 60% of the parasites showed an increase in $[Ca^{2+}]_i$ in response to CPA, and 90% gave an $[Ca^{2+}]_i$ increase upon subsequent **CP2** addition. The percentage of cells that responded to both CPA and **CP2** was ~70% (Fig. 9b).

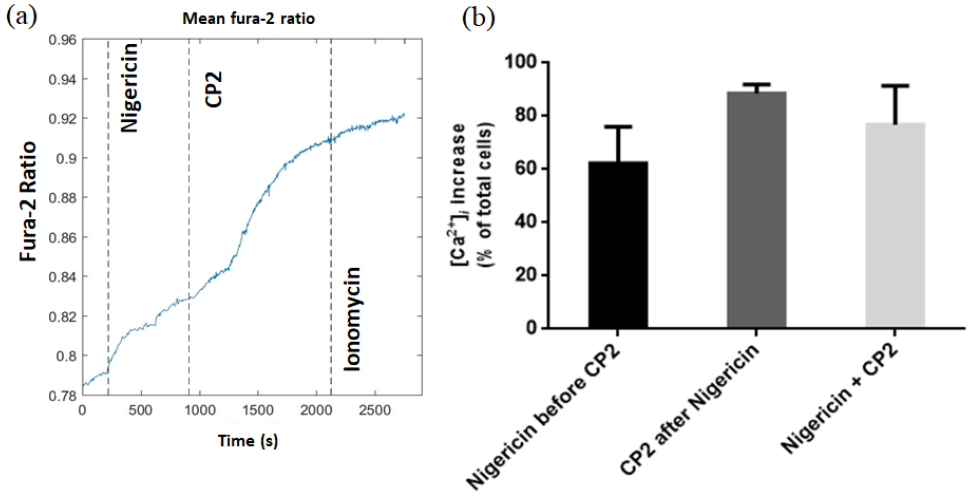

371

372 **Fig. 8**. Effects of **CP2** on $[Ca^{2+}]_i$ in *Leishmania mexicana* after the addition of nigericin.
373 (a) Representative experiment of promastigotes treated with 2.5 µmol L^{-1} nigericin,
374 followed by 7.5 µmol L^{-1} **CP2** and 10 µmol L^{-1} ionomycin. The trace shows an average
375 of at least 100 individual parasites. (b) Mean percentage of parasites with a change in
376 $[Ca^{2+}]_i$ in the presence of nigericin, subsequent **CP2** addition, and those that responded to
377 both nigericin and **CP2**. Data are mean ± SD of three independent experiments. There are
378 no statistically significant differences between groups determined by the one-way
379 ANOVA multiple comparisons test ($p < 0.05$).

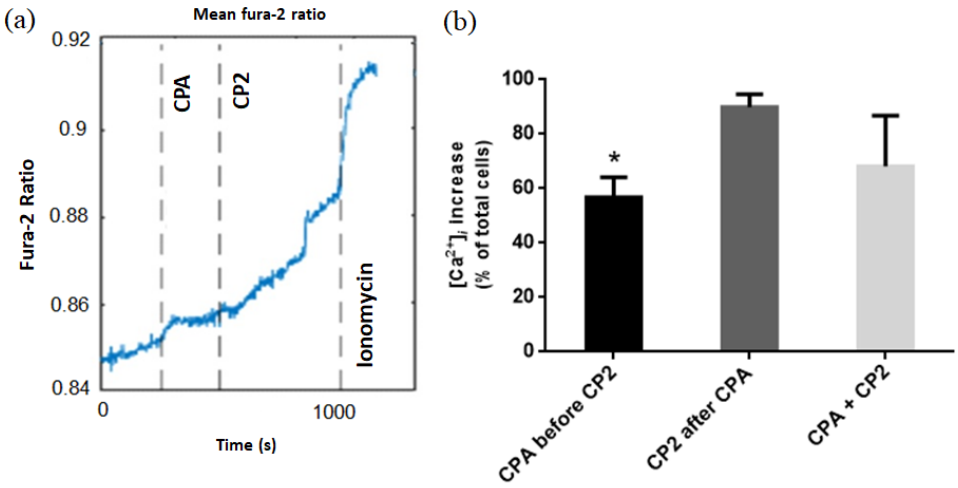

Fig. 9. Effects of **CP2** on $[Ca^{2+}]_i$ in *Leishmania mexicana* after the addition of cyclopiazonic acid (CPA). (a) Representative experiment of promastigotes treated with 10 µmol L^{-1} CPA, followed by 7.5 µmol L^{-1} **CP2** and 10 µmol L^{-1} ionomycin. The trace shows an average of at least 100 individual parasites. (b) Mean of the percentage of parasites with increases in $[Ca^{2+}]_i$ in the presence of CPA, subsequent addition of **CP2,** and those that respond to both CPA and **CP2**. Data are mean ± SD of three independent experiments. *: statistically significant differences relative to **CP2** after CPA addition ($p < 0.05$) were determined by one-way ANOVA multiple comparisons test.

The results described above indicate that the **CP2**-dependent elevation of intracellular Ca^{2+} is not due to release from acidocalcisomes or the ER. To determine whether mitochondria might be the Ca^{2+} source, promastigotes were exposed to **CP2** and the mitochondrial uncoupler FCCP (Fig. 10). The cell percentage with an $[Ca^{2+}]_i$ increase in response to **CP2** was significantly decreased to about 10% by the pre-treatment with FCCP (Fig. 10b). Similarly, prior treatment with **CP2** decreased the response to subsequent FCCP addition. In both sequential addition paradigms, the percentage of

parasites that responded to both FCCP and **CP2** was only ~5% (addition of FCCP followed by **CP2** or **CP2** followed by FCCP). Thus, these data suggest that **CP2** is mobilizing Ca^{2+} from a mitochondrial pool.

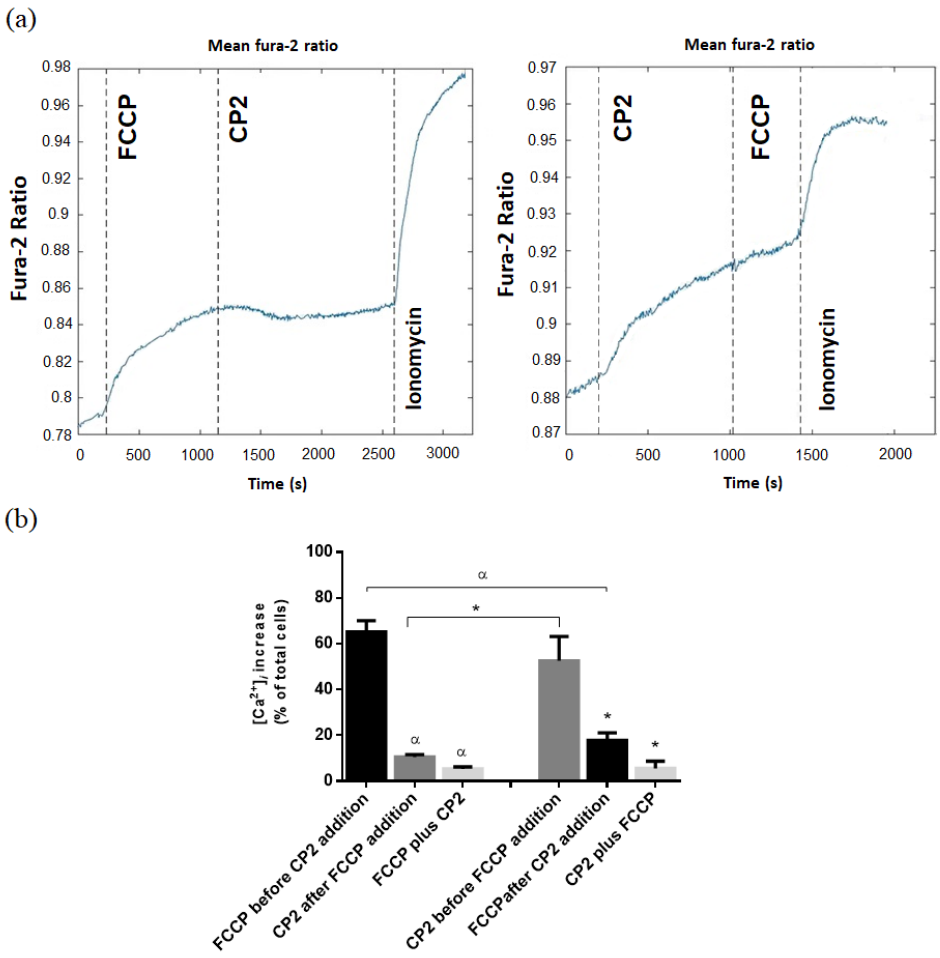

Fig. 10. Effect of **CP2** on the *Leishmania mexicana* $[Ca^{2+}]_i$ before or after addition of FCCP (mitochondrial uncoupler). (a) Representative experiment of promastigotes treated with FCCP followed by **CP2** (5 µmol L^{-1} and 7.5 µmol L^{-1}, respectively) or **CP2** followed by FCCP (7.5 µmol L^{-1} and 5 µmol L^{-1}, respectively), and ionomycin (10 µmol L^{-1}). Each trace is the average from at least 100 individual parasites. (b) Summary data showing mean ± SD of three independent experiments. *: statistically significant difference

relative to cells with $[Ca^{2+}]_i$ increase in the presence of **CP2** ($p < 0.05$); α: statistically significant difference relative to cells with $[Ca^{2+}]_i$ increase in the presence of FCCP ($p < 0.001$) were determined by Two-way ANOVA followed by Tukey's multiple comparisons test.

CP2 depolarized the mitochondrial membrane potential of *Leishmania*

To investigate whether **CP2** alters the mitochondrial membrane potential ($\Delta\psi_m$) of *L. amazonensis*, promastigotes were exposed to different concentrations of **CP2** based on the IC_{50} value for *L. amazonensis* previously determined (30) (IC_{50}: 13.3 µmol L^{-1} and 2 x IC_{50}: 26.6 µmol L^{-1}) for 60 min and changes in $\Delta\psi_m$ were determined with JC-1. The spectrofluorometric data (Fig. 11) showed a decrease in the relative fluorescence intensity in all tested concentrations, indicating the membrane potential's depolarization. Moreover, at a dose of 26.6 µmol L^{-1} of **CP2,** the decrease in the relative fluorescence intensity was similar to that caused by the mitochondrial uncoupler CCCP.

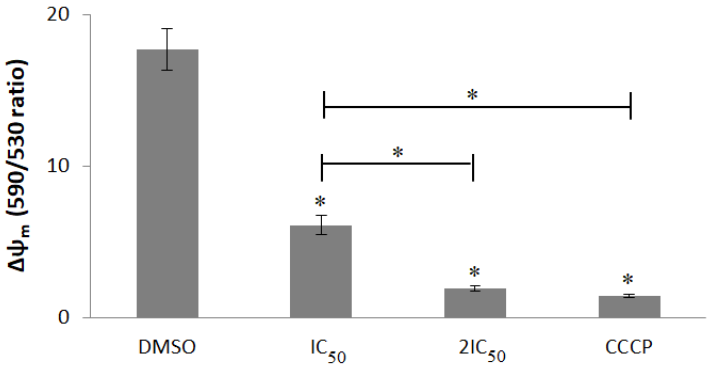

Fig. 11. Analysis of the mitochondrial membrane potential $\Delta\psi_m$ of *L. amazonensis* promastigotes. Promastigotes (2 x 10^6/mL) were incubated with the potential-sensitive probe JC-1 (10 µmol L^{-1}) for 10 min after exposure to different doses of **CP2** (IC_{50}: 13.3

μmol L^{-1} and 2 x IC_{50}: 26.6 μmol L^{-1}) for 60 min or CCCP (50 μmol L^{-1}), 15 min before the addition of JC-1. For the untreated controls, promastigotes were incubated in the presence of 0.1% DMSO. Dose-dependent changes in relative $\Delta\psi_m$ values were expressed as the fluorescence ratio at 590 nm/ 530 nm. *: statistically significant difference relative to the control and between groups ($p < 0.001$). Statistical analysis was determined by ANOVA followed by Student-Newman-Keuls multiple comparisons test.

CP2 causes necrotic parasite death

The cell death mechanism induced by **CP2** was investigated using a dual acridine orange (AO)/ethidium bromide (EB) staining method (Fig. 12) (57). Cultures of *L. amazonensis* promastigotes were exposed to **CP2** for 6, 24, or 48 h, and 200 parasites of each sample were analyzed, and the percentage of viable cells (green), apoptotic-like cells (orange), or necrotic cells (red) calculated (Fig. 12b, 12c, 12d). It was observed that six hours post-**CP2**-treatment (Fig. 12b), promastigotes presented mainly apoptotic-like features (~40%). However, exposure for more extended periods (24 h and 48 h) to **CP2** produced ~50% and 58% necrotic cells, respectively (Fig. 12c and 12d). Cell viability was significantly improved by NAC pre-treatment resulting in the prevention of apoptotic-like and necrotic cells (Fig. 12b-d). These data suggest that **CP2-**induced ROS formation triggers a programmed cell death response.

446

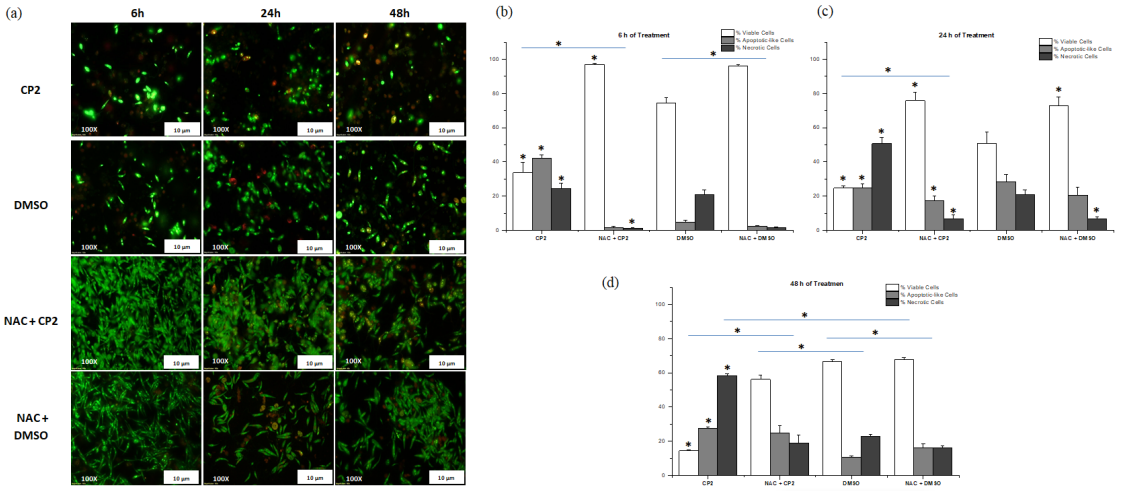

447

448

449

Fig. 12. CP2-induced necrotic cell death in *L. amazonensis*. Promastigotes were treated with 13.3 µmol L^{-1} **CP2** for 6, 24, and 48 h in the presence and absence of 20 µmol L^{-1} NAC pre-treatment for two hours. The parasites were stained with acridine orange and ethidium bromide (AO/EB) and immobilized to be analyzed under a fluorescence microscope, Axio Imager A2 (Zeiss), at 100x magnification. (a) Staining of necrotic / apoptotic-like *L. amazonensis* promastigotes with AO/BE, where viable cells are green, necrotic cells red, and apoptotic-like cells yellow/orange colors. The images were captured with an Axio Cam MRm camera and processed using the AxioVision software. 200 parasites from each sample were evaluated to determine the number of necrotic and apoptotic-like cells after (b) 6 h, (c) 24 h, and (d) 48 h of treatment. 0.1% DMSO was used as a control. Scale, 10 µm. *: statistically significant differences relative to the control and between treatments ($p < 0.001$) were determined by ANOVA with Student-Newman-Keuls multiple comparisons test.

Discussion

We previously reported that the cyclopalladated complex **CP2** inhibits *Leishmania* topoisomerase IB (30), which might lead to DNA damage, triggering cell cycle arrest and DNA repair (58–60). Herein we demonstrated that although **CP2** is a ROS-inducing compound, the observed cell cycle arrest in S-phase, but not cell death, is ROS-independent, unlike DNA damage effects in *T. brucei*, which are ROS inducible (61). Moreover, cells that have sustained DNA damage activate repair proteins, which cause NAD depletion and glycolysis inhibition. As a result, cells that become quickly depleted of ATP suffer necrotic cell death (62). Thus, we hypothesized that **CP2** is causing several and simultaneous deleterious effects on the parasite.

474 Some cyclopalladated compounds act by targeting mitochondria (33, 34, 47, 63). This
475 kind of compound could interact with thiols groups of mitochondrial membrane proteins,
476 causing dissipation of the mitochondrial membrane potential, uncoupling of oxidative
477 phosphorylation, increasing cytosolic Ca^{2+} and decreasing ATP levels, which lead to
478 apoptosis, as reported by Serrano and colleagues (47). In this study, we demonstrated that
479 **CP2** increased ROS and cytosolic Ca^{2+} levels in *Leishmania*.

480 The trypanosomatids mitochondrion is a major source of ROS (64), and in order to deal
481 with oxidative stress, the parasite produces several antioxidant molecules, including
482 glutathione/trypanothione (64–66). Our proteomic analyses revealed other important
483 overexpressed components such as trypanothione reductase and tryparedoxin peroxidase
484 induced by **CP2**. The trypanothione system is unique in trypanosomatids and protects
485 them from oxidative damage and toxic heavy metals (67, 68). The combined action of
486 trypanothione reductase, tryparedoxin, and tryparedoxin peroxidase is central to the
487 maintenance of hydroperoxide metabolism (69). The trypanothione system is related to
488 the mode of action and resistance to drugs containing metals, such as antimonials, by
489 decreasing its thiol buffering capacity in *Leishmania* (68). In addition, elevated ROS
490 levels are associated with increase in peroxiredoxins involved in peroxynitrite protection
491 (70). Thus, high peroxiredoxin levels observed in *Leishmania* after **CP2** exposure might
492 be related to the cell's attempt to stabilize the mitochondrial membrane potential (71);
493 wherein mitochondrial dysfunction and mitochondrial permeability transition induction
494 are candidate intermediate steps in cell death (71, 72).

495 Oxidative membrane alterations can result in a secondary intracellular Ca^{2+} increase
496 responsible for the irreversible disruption of membrane continuity (72). Calcium
497 homeostasis is crucial for the correct functioning of mitochondria, and many
498 antileishmanial agents exert their cytotoxic effects through the disruption of Ca^{2+}

499 homeostasis in the parasite (49, 64). Ca^{2+} is stored in the acidocalcisomes, the ER, and
500 the mitochondrion in trypanosomatids, keeping the cytosolic Ca^{2+} constant. Disruption of
501 cytosolic Ca^{2+} signaling (73) and mitochondrial Ca^{2+} (73) may cause the parasite's death
502 or interfere with its virulence. Ca^{2+} transport mechanisms common to eukaryotic cells
503 operate in the mitochondria of trypanosomatid parasites such as the mitochondrial
504 calcium uniporter (MCU), the voltage-dependent anion channel (VDAC1), and Ca^{2+}/H^{+}
505 exchanger (CHX) (73, 74). VDAC1 in the outer mitochondrial membrane permits the
506 Ca^{2+} influx into the intermembrane space and MCU in the inner mitochondrial membrane
507 transport Ca^{2+} ions into the inner mitochondrial space (75). Efflux of Ca^{2+} to the cytosol
508 from the inner mitochondrial space occurs via the Ca^{2+}/H^{+} exchanger. The transport of
509 Ca^{2+} into the mitochondria is membrane potential-dependent and compounds that perturb
510 the mitochondrial membrane potential result in Ca^{2+} release from the mitochondria into
511 the cytosol as observed for FCCP. We demonstrated that promastigotes treated with **CP2**
512 suffer a loss of mitochondrial membrane potential and release of mitochondrial Ca^{2+} into
513 the cytosol. Our results demonstrated that the high levels of $[Ca^{2+}]_i$ observed in
514 *Leishmania* exposed to **CP2** were derived from the mitochondrion, as a result of the loss
515 of mitochondrial membrane potential.

516 Increased *Leishmania* calreticulin and PDI levels after **CP2** exposure was also observed.
517 Calreticulin is a protein that presents high affinity for Ca^{2+}, contributing to the
518 maintenance of Ca^{2+} homeostasis. However, its Ca^{2+} affinity decreases in the presence of
519 PDI (76), leading to a rapid disturbance in its homeostasis, which can be translated into
520 cell death processes (77, 78).

521 The cyclopalladated compound DPPE 1.1, and not Pd^{2+}, induced mitochondrial
522 permeabilization and elevation in the cytosolic Ca^{2+} levels from intracellular pools, since
523 $PdCl_2$ was not able to promote the same effect on the cation permeabilization (47).

524 Similarly, the heavy metal ion chelator TPEN herein used could not prevent the **CP2**-
525 induced cytosolic Ca^{2+} increase, suggesting that the observed effect was not due to free
526 Pd^{2+}. Additionally, the [Pd(*C*^{2},*N*-dmba)(N_3)] CP2's moiety is important for the Ca^{2+} to
527 unbalance since free dmba was not able to exert an antileishmanial effect (29).

528 Protein folding is sensitive to changes in Ca^{2+} flux and the parasite's exposure to reducing
529 agents (79). Proteins such as HSP70, HSP10, GRP78, and PDI play an important role in
530 repairing the correct three-dimensional structure of unfolded proteins or forming
531 aggregates due to stress. The observed increment of these proteins in **CP2**- treated
532 parasites suggests the parasite's efforts to refold proteins and diminish the harmful effect
533 of **CP2** to the cell. Moreover, GRP78, HSP70, and PDI are dependent on ATPase activity
534 (80) and are strongly related to the increase in proteins secreted inside ER and degraded
535 by the proteasome. The mentioned above will be the subject of analysis in future studies.

536 In trypanosomatids, apoptosis-like cell death mechanisms associated with a lack of
537 molecular markers and conditions are not fully understood (81). It is known that low ROS
538 levels promote apoptosis events, while necrosis is observed at high ROS levels (72, 82–
539 84). Our data showed that *Leishmania* exposed to **CP2** increased ROS levels along 60
540 min, which favored the necrotic process as seen in parasites exposed to **CP2** for 24 h.
541 Moreover, the percentage of living or apoptotic-like promastigotes after **CP2** exposure
542 increased in the presence of NAC. Indeed, in our previous work (30), it was reported an
543 inflammatory process in a *L. amazonensis*-infected BALB/c mice treated with **CP2**,
544 which might corroborate the high number of necrotic cells herein detected after parasite
545 exposure to **CP2** for 48h.

546 It is important to consider that Ca^{2+} also plays an important role in cell death mechanisms
547 inducing both apoptosis (Ca^{2+} low levels) or necrosis (Ca^{2+} high levels) (72, 82, 84). We
548 have shown here that promastigotes exposed to **CP2** displayed changes in $[Ca^{2+}]_i$,

followed by cell death. Thus, high ROS and $[Ca^{2+}]_i$ levels were observed ~10 min after **CP2** addition, which suggested that ROS production is shortly followed by release of mitochondrial Ca^{2+}. These data suggest that ROS might be playing an essential role in the signaling/execution of the observed cell death mechanism and that Ca^{2+} acts onto the observed mitochondrial changes, such as membrane depolarization, pointing out the parasite mitochondrion as central in orchestrating cell fate after triggering cell death signaling induced by **CP2** (34, 49, 85).

Finally, beyond the antileishmanial efficacy previously reported by **CP2** in a CL mice model (30), herein, we demonstrated that **CP2** is also able to diminish the parasite load in a hamsters model, as a visceral leishmaniasis model, indicating the broadly potential of **CP2** to exert its antileishmanial activity targeting other leishmaniasis clinical manifestations. Thus, this work herein presented will help to promote rational drug modifications and thus contribute to the pipeline of leishmaniasis drug discovery.

MATERIALS AND METHODS

Compounds

The binuclear cyclopalladated complex $[Pd(C^2,N\text{-dmba})(\mu\text{-}N_3)]_2$ (dmba: N,N-dimethylbenzylamine), here denominated **CP2**, was obtained as previously described (86). Stock solutions of **CP2**, amphotericin B - AmpB (Cristalia, São Paulo, Brazil), nigericin (Sigma – Aldrich), FCCP (Sigma – Aldrich), ionomycin (Sigma – Aldrich), CPA (Calbiochem; San Diego, CA) and, TPEN (Sigma – Aldrich) were dissolved in dimethylsulfoxide (DMSO) (Sigma – Aldrich) and further diluted in culture media (final 0.1 % DMSO). Stock solutions were kept at -20°C.

Biological Assay

Parasites culture

Promastigotes of *L. mexicana* strain MNYC/BZ/62/M379 and *L. infantum* strain MHOM/BR/1972/LD were maintained in Schneider's Insect medium (Sigma – Aldrich) and *L. amazonensis* strain MPRO/BR/1972/M1841-LV-79 was maintained in liver-infusion tryptose (LIT) medium (87) at 28°C, supplemented with 10% heat-inactivated bovine serum (iFBS; Gibco/Invitrogen) and 1% penicillin/streptomycin (Sigma – Aldrich).

Animals

Male Swiss albino mice used to evaluate *in vitro* leishmanicidal activity against intracellular amastigotes were obtained from São Paulo State University (UNESP, Araraquara, São Paulo, Brazil). Male Golden hamsters (*Mesocricetus auratus*) used in *in vivo* assays were acquired from ANILAB (Animais de Laboratório Criação e Comércio Ltda, Paulínia, São Paulo, Brazil). All animals were maintained in single-sex cages under a 12-h light/12-h dark cycle in a controlled temperature room (22 ± 2°C), and they were fed *ad libitum*. The Ethics Committee approved this study for Animal Experimentation of São Paulo State University (UNESP), the School of Pharmaceutical Sciences (CEUA/FCF/CAr, 18/2015 and 44/2015) in agreement with the guidelines of Sociedade Brasileira de Ciência de Animais de Laboratório (SBCAL) and Conselho Nacional de Controle da Experimentação Animal (CONCEA).

Antileishmanial *in vivo* assay

To analyze the potential spectrum of action of **CP2**, we evaluated *in vitro* and *in vivo* leishmanicidal activity of the cyclopalladated against *L. infantum*. The MTT assay

evaluated the susceptibility of *L. infantum* promastigotes, and evaluation of intracellular amastigotes forms was made according to previously reported methodology (29, 30); followed by evaluation of *in vivo* leishmanicidal activity of **CP2** against *L. infantum*-infected hamsters according to previously established methodology (88). Briefly, eight-week-old male golden hamsters were intraperitoneally infected with $2x10^8$ promastigotes of *L. infantum* in the stationary phase of growth and randomly separated into six groups containing five animals per cage. Seventy days post-infection, the animals received 15 daily intraperitoneal doses of **CP2** (1.5 or 0.75 mg/Kg/day), the reference drug AmpB (20 mg/Kg/day), or PBS (vehicle); untreated infected animals and non-infected animals were also evaluated. The animals were euthanized at the end of treatment. According to previously established methodology, the blood was collected by cardiac puncture to obtain blood serum samples to analyze liver and renal function biomarkers (88). Parasite burden in the spleen and liver was determined by limiting dilution methodology as previously described (88, 89).

Proteomic Analyses

For comparative proteomic analysis, $1x10^7$ parasites mL^{-1} of promastigote forms of *L. amazonensis* in the mid-log phase were treated with 13.3 µmol L^{-1} **CP2** (IC_{50} of **CP2** previously reported) (30) for 72 h. The extraction of total proteins of promastigotes was carried out in the presence (treated cells) and absence of **CP2** (untreated cells). The parasite cultures were made in biological triplicates.

Protein Extraction

Promastigote forms of *L. amazonensis* untreated and treated with **CP2** were centrifuged at 2,000 *g* for 10 min at 4°C. The pellet was washed three times with tryps wash (100 mmol L^{-1} NaCl, 3 mmol L^{-1} $MgCl_2$, 20 mmol L^{-1} Tris-HCl, pH 7.5) and resuspended in 500 µL of lysis solution (7 mol L^{-1} urea, 2 mol L^{-1} thiourea, 4% CHAPS, 2% IPG buffer 3-10, 40 mmol L^{-1} DTT) (90) containing a protease inhibitor cocktail (cOmplete™, Mini Protease Inhibitor Cocktail, Roche) for one hour under constant stirring at 4°C. Finally, the supernatant was collected by centrifugation at 14,000 *g* for 3 min at 4°C and stored at -80°C until the time of use. Protein extract quantification was performed with the 2D Quant Kit (GE Healthcare) using the Infinite 200 pro plate reader (TECAN).

Two-dimensional SDS-PAGE

2D gels were run in triplicate according to standard procedures. pH 4–7 IPG buffer (Sigma– Aldrich) and bromophenol blue were added to 61.5 µg of protein and ran on 24 cm pH 4–7 strips (GE Healthcare). Strips were equilibrated in equilibration buffer (6 mol L^{-1} urea, 75 mmol L^{-1} Tris-HCl pH 8.8, 29.3% glycerol, 2% SDS, 0.002% bromophenol blue) containing 25 mg mL^{-1} dithiothreitol (DTT) for 15 min under gentle stirring. The previous solution was discarded, and a new equilibration buffer containing 10 mg mL^{-1} iodoacetamide was added for 15 min. For the first dimension, rehydrated strips containing protein extracts of *L. amazonensis* promastigotes were transferred to ceramic support (Ettan IPGphor Manifold - GE Healthcare) and subjected to 50 µA per strip for protein migration using the Ettan IPGphor II Isoelectric Focusing System (GE Healthcare). The second dimension was run on 12.5% polyacrylamide gels (40 mA per gel) under continuous cooling (10°C) using a *SE 600 Ruby* and Multitemp IV (GE Healthcare). The gels were stained with 0.1% Phast Gel Blue R solution (GE Healthcare) before scanning and analysis using ImageMaster™ 2D Platinum 7.0 software (GE Healthcare). Spots were

cut, destained, and dried before trypsinization. Briefly, the spots were washed three times using a 0.1 mol L^{-1} NH_4HCO_3 in 50% acetonitrile (ACN), followed by the addition of pure ACN for 15 min. Finally, the spots were air-dried and trypsinized with Trypsin Gold mass spectrometry grade (Promega) according to the manufacturer's instructions.

Mass Spectrometry (MS) Analysis

The analysis of tryptic peptides was performed in the nanoACQUITY UPLC (Waters, Milliford, USA) coupled to the mass spectrometer Xevo Q-TOF G2 (Waters, Milliford, USA). For this, the UPLC nanoACQUITY system was equipped with a column of HSS T3 (Acquity UPLC HSS T3 column 75 mm x 150 mm; 1.8 µm, Waters), previously equilibrated with 7% of the mobile phase B (100% ACN + 0.1% formic acid). The peptides were separated by a linear gradient of 7% to 85% of mobile phase B for 20 min with 0.35 µL min^{-1} of flow and 45°C. MS was operated in positive ion mode, with a data acquisition time of 20 min. The data obtained were processed using ProteinLynx GlobalServer 3.0 software (PLGS) (Waters, Milliford, USA). Protein identification of *L. amazonensis* was performed using the ion count algorithm integrated with the software and searched against the *Leishmania mexicana* UniProt (Universal Protein Resource, http://www.uniprot.org/proteomes/?query=Leishmania&sort=score, proteome ID UP000007259) protein database (analysis date: March 2016)), used for comparison purposes since *L. amazonensis* and *L. mexicana* are phylogenetically related (6, 7, 91).

Cell Cycle Analysis

Promastigotes of *L. amazonensis* were grown in a LIT medium at 28ºC. Parasites in the exponential phase of growth ($3x10^6$ parasites mL^{-1}) were incubated with 5 mmol L^{-1}

hydroxyurea (HU) for eight hours and then transferred to HU-free medium supplemented with 0.03% DMSO, 20 µmol L^{-1} NAC (N-Acetyl-L-cysteine, Sigma), 53.2 or 133 µmol L^{-1} **CP2** (4 x IC_{50} or 10 x IC_{50}), 20 µmol L^{-1} NAC + 53.2 or 133 µmol L^{-1} **CP2**. Cells were collected after 2, 4, 6, or 8 h of treatment, washed with 1X PBS and fixed in 30% PBS/70% methanol overnight at 4°C. Fixed cells were washed with 1X PBS and stained with PBS solution containing propidium iodide (10 µg mL^{-1}) and RNase A (10 µg mL^{-1}) at 37°C for 30 min. Flow cytometry data were collected using the BD FACSCanto1 flow cytometer. Data were analyzed using FlowJo software.

Intracellular ROS measurement

Intracellular ROS levels were compared after *L. amazonensis* exposure to **CP2** based on the methodology previously described with some modifications (92). Briefly, parasites cultivated in Schneider's Insect medium until the mid-log growth phase were harvested, washed, and resuspended in modified 1X HBSS (Hank's Balanced Salts, Sigma) medium containing 1.3 mmol L^{-1} $CaCl_2$. Then, $1x10^7$ promastigotes mL^{-1} were incubated in the dark with 20 mmol L^{-1} H_2DCFDA (2',7'-dichlorodihydrofluorescein diacetate, Sigma) for 30 min followed by treatment with different concentrations of **CP2** based on the previously determined IC_{50} value as follows (30): 6.7 µmol L^{-1} (½ x IC_{50}), 13.3 µmol L^{-1} (1 x IC_{50}), 26.6 µmol L^{-1} (2 x IC_{50}), and 53.2 µmol L^{-1} (4 x IC_{50}). A volume of 200 µL of parasites was transferred to the wells of black bottom plates, and the fluorescence was measured at 530 nm (emission), and 480 nm (excitation) for 60 min (Infinite 200, TECAN) and the basal fluorescence subtracted at the end of the process.

Live-cell Fura-2 Ca^{2+} imaging

Promastigotes of *L. mexicana* in the mid-log phase ($1x10^7$ parasites mL^{-1}) were harvested and subsequently washed in loading buffer (8.5 mmol L^{-1} Na_2HPO_4, 1.5 mmol L^{-1} KH_2PO_4, 137 mmol L^{-1} NaCl, 4 mmol L^{-1} KCl, 10 mmol L^{-1} HEPES 0.8 mmol L^{-1} $MgCl_2$, 0.8 mmol L^{-1} $MgSO_4$, 5 mmol L^{-1} glucose, 2.4 mmol L^{-1} probenecid, pH 7.4), with and without 1.3 mmol L^{-1} $CaCl_2$, that contained 5 µmol L^{-1} Fura-2/AM (2-{6-[Bis(carboxymethyl)amino]-5-(2-{2-[bis(carboxymethyl)amino]-5-methylphenoxy}ethoxy)-1-benzofuran-2-yl}-1,3-oxazole-5-carboxylic acid, Molecular Probes, Eugene, OR) and 2 µmol L^{-1} pluronic acid F-127 (Molecular Probes, Eugene, OR). The suspensions were incubated for two hours at 28°C in the dark. Parasites were washed twice with the loading buffer to remove the extracellular dye and immobilized on coverslips previously treated with 2 µL *Cell Tak* (Corning® Cell-Tak Cell and Tissue Adhesive) for 5 min. The coverslip containing the immobilized cells was transferred to the microscope stage (*thermostatically regulated microscope chamber,* Open Perfusion Micro-Incubator (PDMI-2)) at 28°C. The fluorescence of promastigote forms loaded with Fura-2/AM was captured at 40x magnification, using an inverted microscope *Nikon Eclipse TE300* (Nikon, Melville, NY) has coupled to a digital camera *Hamamatsu EM-CCD Imagem.* Image acquisition was performed every 3 s at 340 nm and 380 nm excitation and 510 nm emission. A series of images generated in-frame was transformed into a video with the software NIS-Elements AR 4.20.02. The results were obtained from at least three independent experiments of 100 promastigote forms per assay. Responses to the addition of different compounds were captured in real-time, followed by 10 µmol L^{-1} ionomycin to determine maximal fluorescence.

Measurement of the mitochondrial transmembrane potential $\Delta\psi_m$

Changes in the $\Delta\psi_m$ were measured spectrofluorimetrically using the cationic lipophilic dye 5,5′,6,6′-tetrachloro-1,1′,3,3′-tetraethylbenzimidazole carbocyanide iodide (JC-1) (Sigma – Aldrich). Briefly, $2x10^6$ promastigotes mL^{-1} of *L. amazonensis* were cultured for 60 min in the presence or absence of **CP2**. The parasites were harvested, resuspended in HBSS containing 1.3 mmol L^{-1} $CaCl_2$, and incubated with JC-1 (10 µmol L^{-1}) for 10 min at 28°C. For positive control, 50 µmol L^{-1} of the mitochondrial uncoupler carbonyl cyanide 3-chlorophenylhydrazone (CCCP) was added to untreated control cells 15 min before addition of JC-1. After washing twice with HBSS, fluorescence was measured at 530 nm and 590 nm using a spectrofluorometer (TECAN) with an excitation wavelength of 485 nm. The 590 nm/ 530 nm ratio values were plotted as the relative $\Delta\psi_m$ (93).

Cell death analysis using acridine orange/ethidium bromide (AO/EB) staining

Promastigotes of *L. amazonensis* in the mid-log phase ($1x10^7$ parasites mL^{-1}) were incubated with 13.3 µmol L^{-1} **CP2** for 6 h, 24 h, and 48 h. Likewise, parasites were incubated with 0.1% DMSO as a control. Besides, parasites were pre-treated with 20 µmol L^{-1} NAC for two hours before **CP2** addition. After the incubation period, the parasites were centrifuged for 10 min at 2,000 *g* and washed with PBS, and resuspended in 200 µL of PBS. 20 µL of cell suspension were stained with a mixture of ethidium bromide and acridine orange (100 µg mL^{-1}) and immobilized on a glass coverslip previously treated with *Cell Tak*, as described above. The labeled parasites were visualized by fluorescence microscopy (Axioplan-Zeiss) with 100x magnification and a FITC filter (460-490 nm band-pass excitation filter and 510-560 nm emission) according to a previously described methodology (57). For the percentage quantification of each event, 200 cells from each sample were counted.

742 **Statistical Analysis**

743 The biological assays' data were analyzed by one-way analysis of variance (ANOVA)
744 followed by Tukey and Student-Newman-Keuls Multiple Comparisons Test (Graph Pad
745 InStat software and GraphPad Prism software). Differences were considered significant
746 when $p \leq 0.05$.

747

748

749 **ACKNOWLEDGMENTS**

750 This work was supported by the São Paulo Research Foundation (FAPESP) grants:
751 #2016/05345-4, #2016/177115, #2017/03552-5 and #2018/23015-7; Programa de Apoio
752 ao Desenvolvimento Científico da Faculdade de Ciências Farmacêuticas da UNESP
753 (PADC); and Funding from the Thomas P. Infusino Endowment at Rutgers University.
754 AMAV (#2016/19289-9 and #2019/21661-1) and SV (#2016/18191-5) were supported
755 by FAPESP. This study was financed in part by the Coordenação de Aperfeiçoamento de
756 Pessoal de Nível Superior - Brasil (CAPES) - Finance Code 001, IAPL, TGP, KBI, JMV.
757 MARB, AVGN and MASG are recipienu of a Research Productivity Scholarship from
758 the National Council for Research and Development (CNPq). We thank Prof. Dr. Janice
759 Rodrigues Perussi, from USP – São Carlos, for kindly allowing us to have access to the
760 fluorescence microscope, and "Núcleo de atendimento à comunidade (NAC), FCF,
761 UNESP," for the analysis of biomarkers of liver and renal function. The funders had no
762 role in study design, data collection, analysis, decision to publish, or manuscript
763 preparation.

764

765 **AUTHOR CONTRIBUTIONS**

AMAV, LROT, APT, and MASG designed the studies. JMV and AVGN synthesized the cyclopalladated complex CP2. AMAV, IAPL, TGP, DD, KBI, SV, and ALL performed the experiments and acquired the data. AMAV, PJB, IAPL, TGP, DD, KBI, SV, LROT, MARB, AVG, APT, and MASG contributed to the data analysis and interpretation results. AMAV wrote the manuscript. AMAV, PJB, LROT, MARB, APT, and MASG reviewed and edited the manuscript.

DECLARATION OF INTERESTS

The authors declare no conflict of interest.

REFERENCES

1. **Burza S**, **Croft SL**, **Boelaert M**. 2018. Leishmaniasis. Lancet **392**:951–970.
2. **Barrett MP**, **Croft SL**. 2012. Management of trypanosomiasis and leishmaniasis. Br Med Bull **104**:175–196.
3. **Lindoso JAL**, **Cunha MA**, **Queiroz IT**, **Moreira CHV**. 2016. Leishmaniasis – HIV coinfection: current challenges. Dovepress **8**:147–156.
4. **Monzote L**. 2009. Current Treatment of Leishmaniasis: A Review. Open Antimicrob Agents J **1**:9–19.
5. **Herwaldt BL**. 1999. Leishmaniasis. Lancet **354**:1191–1199.
6. **Silveira FT**, **Lainson R**, **Corbett CEP**. 2004. Clinical and immunopathological spectrum of American cutaneous leishmaniasis with special reference to the disease in Amazonian Brazil: a review. Mem Inst Oswaldo Cruz **99**:239–251.
7. **Mann S**, **Frasca K**, **Scherrer S**, **Henao-martínez AF**, **Newman S**, **Ramanan P**,

Suarez JA. 2021. A Review of Leishmaniasis : Current Knowledge and Future Directions. Curr Trop Med Reports **8**:121–132.

8. **Singh N**, **Kumar M**, **Singh RK**. 2012. Leishmaniasis: Current status of available drugs and new potential drug targets. Asian Pac J Trop Med **5**:485–497.

9. **Van Griensven J**, **Diro E**. 2012. Visceral Leishmaniasis. Infect Dis Clin North Am **26**:309–322.

10. **Croft SL**, **Sundar S**, **Fairlamb AH**. 2006. Drug resistance in leishmaniasis. Clin Microbiol Rev **19**:111–126.

11. **Meheus F**, **Balasegaram M**, **Olliaro P**, **Sundar S**, **Rijal S**, **Faiz MA**, **Boelaert M**. 2010. Cost-Effectiveness Analysis of Combination Therapies for Visceral Leishmaniasis in the Indian Subcontinent. PLoS Negl Trop Dis **4**:e818.

12. **Palumbo E**. 2009. Current treatment for cutaneous leishmaniasis: a review. Am J Ther **16**:178–182.

13. **Katsuno K**, **Burrows JN**, **Duncan K**, **van Huijsduijnen RH**, **Kaneko T**, **Kita K**, **Mowbray CE**, **Schmatz D**, **Warner P**, **Slingsby BT**. 2015. Hit and lead criteria in drug discovery for infectious diseases of the developing world. Nat Rev Drug Discov **14**:751–758.

14. **Chawla B**, **Madhubala R**. 2010. Drug targets in Leishmania. J Parasit Dis **34**:1–13.

15. **Siqueira-Neto JL**, **Song O-R**, **Oh H**, **Sohn J-H**, **Yang G**, **Nam J**, **Jang J**, **Cechetto J**, **Lee CB**, **Moon S**, **Genovesio A**, **Chatelain E**, **Christophe T**, **Freitas-Junior LH**. 2010. Antileishmanial High-Throughput Drug Screening Reveals Drug Candidates with New Scaffolds. PLoS Negl Trop Dis **4**:e675.

16. **Freitas-Junior LH**, **Chatelain E**, **Kim HA**, **Siqueira-Neto JL**. 2012. Visceral leishmaniasis treatment: What do we have, what do we need and how to deliver it? Int J Parasitol Drugs drug Resist **2**:11–19.

17. **Akbari M**, **Oryan A**, **Hatam G**. 2017. Application of nanotechnology in treatment of leishmaniasis : A Review. Acta Trop **172**:86–90.

18. **De Almeida L**, **Fujimura AT**, **Del Cistia ML**, **Fonseca-Santos B**, **Imamura KB**, **Michels PAM**, **Chorilli M**, **Graminha MAS**. 2017. Nanotechnological Strategies for Treatment of Leishmaniasis — A Review. J Biomed Nanotechnol **13**:117–133.

19. **Torres FAE**, **Passalacqua TG**, **Velásquez AMA**, **de Souza RA**, **Colepicolo P**, **Graminha MAS**. 2014. New drugs with antiprotozoal activity from marine Algae: A review. Brazilian J Pharmacogn **24**:265–276.

20. **Falkenberg M**, **Nakano E**, **Zambotti-Villela L**, **Zatelli GA**, **Philippus AC**, **Imamura KB**, **Velasquez AMA**, **Freitas RP**, **Tallarico LDF**, **Colepicolo P**, **Graminha MAS**. 2018. Bioactive compounds against neglected diseases isolated from macroalgae : a review. J Appl Phycol.

21. **Elgazwy A-SSH**, **Ismail NSM**, **Atta-Allah SR**, **Sarg MT**, **Soliman DHS**, **Zaki MY**, **Elgamas MA**. 2012. Palladacycles as Antimicrobial Agents. Curr Med Chem **19**:3967–3981.

22. **Anilanmert B**. 2012. Therapeutic Organometallic Compounds, p. 651–680. *In* Galleli, L (ed.), Pharmacologyintech. croatia.

23. **Farrell N**. 2003. Metal Complexes as Drugs and Chemotherapeutic Agents, p. 809–840. *In* Comprehensive Coordination Chemistry IIElsevier L. Elsevier Ltd., USA.

24. **Sánchez-Delgado RA**, **Anzellotti A**. 2004. Metal complexes as chemotherapeutic agents against tropical diseases: trypanosomiasis, malaria and leishmaniasis. Mini-Reviews Med Chem **4**:23–30.

25. **Fricker SP**, **Mosi RM**, **Cameron BR**, **Baird I**, **Zhu Y**, **Anastassov V**, **Cox J**, **Doyle PS**, **Hansell E**, **Lau G**, **Langille J**, **Olsen M**, **Qin L**, **Skerlj R**, **Wong RSY**, **Santucci Z**, **McKerrow JH**. 2008. Metal compounds for the treatment of parasitic diseases. J Inorg Biochem **102**:1839–1845.

26. **Navarro M**, **Gabbiani C**, **Messori L**, **Gambino D**. 2010. Metal-based drugs for malaria, trypanosomiasis and leishmaniasis: Recent achievements and perspectives. Drug Discov Today **15**:1070–1078.

27. **Lopera AA**, **Velásquez AMA**, **Clementino LC**, **Robledo S**, **Montoya A**, **de Freitas LM**, **Bezzon VDN**, **Fontana CR**, **Garcia C**, **Graminha MAS**. 2018. Solution-combustion synthesis of doped TiO2 compounds compounds and its potential antileishmanial activity mediated by photodynamic therapy. J Photochem Photobiol B Biol **183**:64–74.

28. **Velásquez AMA**, **Francisco AI**, **Kohatsu AAN**, **Silva FA de J**, **Rodrigues DF**, **Teixeira RG da S**, **Chiari BG**, **de Almeida MGJ**, **Isaac VLB**, **Vargas MD**, **Cicarelli RMB**. 2014. Synthesis and tripanocidal activity of ferrocenyl and benzyl diamines against Trypanosoma brucei and Trypanosoma cruzi. Bioorg Med Chem Lett **24**:1707–1710.

29. **Velásquez AMA**, **de Souza RA**, **Passalacqua TG**, **Ribeiro AR**, **Scontri M**, **Chin CM**, **de Almeida L**, **Del Cistia ML**, **da Rosa JA**, **Mauro AE**, **Graminha MAS**. 2016. Antiprotozoal activity of the cyclopalladated complexes against Leishmania amazonensis and Trypanosoma cruzi. J Braz Chem Soc **27**:1032–

1039.

30. **Velásquez AMA**, **Ribeiro WC**, **Venn V**, **Castelli S**, **Camargo MS de**, **de Assis RP**, **de Souza RA**, **Ribeiro AR**, **Passalacqua TG**, **da Rosa JA**, **Baviera AM**, **Mauro AE**, **Desideri A**, **Almeida-Amaral EE**, **Graminha MAS**. 2017. Efficacy of a Binuclear Cyclopalladated Compound Therapy for Cutaneous Leishmaniasis in the Murine Model of Infection with Leishmania amazonensis and Its Inhibitory Effect on Topoisomerase 1B. Antimicrob Agents Chemother **61**:e00688-17.

31. **Clementino L da C**, **Velásquez AMA**, **Passalacqua TG**, **de Almeida L**, **Graminha MAS**, **Martins GZ**, **Salgueiro L**, **Cavaleiro C**, **Sousa M do C**, **Moreira RRD**. 2018. In vitro activities of glycoalkaloids from the Solanum lycocarpum against Leishmania infantum. Brazilian J Pharmacogn **28**:673–677.

32. **Passalacqua TG**, **Dutra LA**, **de Almeida L**, **Velásquez AMA**, **Torres FAE**, **Yamasaki PR**, **dos Santos MB**, **Regasini LO**, **Michels PAM**, **Bolzani V da S**, **Graminha MAS**. 2015. Synthesis and evaluation of novel prenylated chalcone derivatives as anti-leishmanial and anti-trypanosomal compounds. Bioorganic Med Chem Lett **25**:3342–3345.

33. **Matsuo AL**, **Silva LS**, **Torrecilhas AC**, **Pascoalino BS**, **Ramos TC**, **Rodrigues EG**, **Schenkman S**, **Caires ACF**, **Travassos LR**. 2010. In vitro and in vivo trypanocidal effects of the cyclopalladated compound 7a, a drug candidate for treatment of Chagas' disease. Antimicrob Agents Chemother **54**:3318–3325.

34. **Arruda DC**, **Matsuo AL**, **Silva LS**, **Real F**, **Leitão NP**, **Pires JHS**, **Caires ACF**, **Garcia DM**, **Cunha FFM**, **Puccia R**, **Longo LVG**. 2015. Cyclopalladated Compound 7a Induces Apoptosis- and Autophagy-Like Mechanisms in Paracoccidioides and Is a Candidate for Paracoccidioidomycosis Treatment.

884 Antimicrob Agents Chemother **59**:7214–7223.

885 35. **Paladi CDS**, **Pimentel IAS**, **Katz S**, **Cunha RLOR**, **Judice WA de S**, **Caires**
886 **ACF**, **Barbiéri CL**. 2012. In vitro and In vivo activity of a palladacycle complex
887 on Leishmania (Leishmania) amazonensis. PLoS Negl Trop Dis **6**:e1626.

888 36. **Paladi CS**, **da Silva DAM**, **Motta PD**, **Garcia DM**, **Teixeira D**, **Longo-**
889 **Maugéri IM**, **Katz S**, **Barbiéri CL**. 2017. Treatment of Leishmania
890 (Leishmania) Amazonensis -Infected Mice with a Combination of a Palladacycle
891 Complex and Heat-Killed Propionibacterium acnes Triggers Protective Cellular
892 Immune Responses. Front Microbiol **8**:1–11.

893 37. **Dos Santos IB**, **da Silva DAM**, **Paz FACR**, **Garcia DM**, **Carmona AK**,
894 **Teixeira D**, **Longo-Maugéri IM**, **Katz S**, **Barbiéri CL**. 2018. Leishmanicidal
895 and Immunomodulatory Activities of the Palladacycle Complex DPPE 1.1, a
896 Potential Candidate for Treatment of Cutaneous Leishmaniasis. Front Microbiol
897 **9**:1–9.

898 38. **Vieites M**, **Otero L**, **Santos D**, **Toloza J**, **Figueroa R**, **Norambuena E**, **Olea-**
899 **Azar C**, **Aguirre G**, **Cerecetto H**, **González M**, **Morello A**, **Maya JD**, **Garat**
900 **B**, **Gambino D**. 2008. Platinum(II) metal complexes as potential anti-
901 Trypanosoma cruzi agents. J Inorg Biochem **102**:1033–1043.

902 39. **Navarro M**, **Hernández C**, **Colmenares I**, **Hernández P**, **Fernández M**,
903 **Sierraalta A**, **Marchán E**. 2007. Synthesis and characterization of
904 [Au(dppz)2]Cl3 . DNA interaction studies and biological activity against
905 Leishmania (L) mexicana. J Inorg Biochem **101**:111–116.

906 40. **Zinsstag J**, **Brun R**, **Craciunescu DG**, **Parrondo Iglesias E**. 1991. In vitro
907 activity of organometallic complexes of Ir, Pt and Rh on Trypanosoma b.

gambiense, T. b. rhodesiense and T. b. brucei. Trop Med Parasitol Off organ Dtsch Tropenmedizinische Gesellschaft Dtsch Gesellschaft fur Tech Zusammenarbeit **42**:41–44.

41. **Croft SL**, **Neal RA**, **Craciunescu DG**, **Certad-Fombona G**. 1992. The activity of platinum, iridium and rhodium drug complexes against Leishmania donovani. Trop Med Parasitol **43**:24–28.

42. **Santos D**, **Parajón-Costa B**, **Rossi M**, **Caruso F**, **Benítez D**, **Varela J**, **Cerecetto H**, **González M**, **Gómez N**, **Caputto ME**, **Moglioni AG**, **Moltrasio GY**, **Finkielsztein LM**, **Gambino D**. 2012. Activity on Trypanosoma cruzi, erythrocytes lysis and biologically relevant physicochemical properties of Pd(II) and Pt(II) complexes of thiosemicarbazones derived from 1-indanones. J Inorg Biochem **117**:270–276.

43. **Otero L**, **Vieites M**, **Boiani L**, **Denicola A**, **Rigol C**, **Opazo L**, **Olea-Azar C**, **Maya JD**, **Morello A**, **Krauth-Siegel RL**, **Piro OE**, **Castellano E**, **González M**, **Gambino D**, **Cerecetto H**. 2006. Novel antitrypanosomal agents based on palladium nitrofurylthiosemicarbazone complexes: DNA and redox metabolism as potential therapeutic targets. J Med Chem **49**:3322–3331.

44. **Franco LP**, **de Góis EP**, **Codonho BS**, **Pavan ALR**, **Pereira I de O**, **Marques MJ**, **de Almeida ET**. 2013. Palladium(II) imine ligands cyclometallated complexes with a potential leishmanicidal activity on Leishmania (L.) amazonensis. Med Chem Res **22**:1049–1056.

45. **Bjelogrlić SK**, **Todorović TR**, **Kojić M**, **Senćanski M**, **Nikolić M**, **Višnjevac A**, **Araškov J**, **Miljković M**, **Muller CD**, **Filipović NR**. 2019. Pd (II) complexes with N-heteroaromatic hydrazone ligands: Anticancer activity, in silico and

experimental target identification. J Inorg Biochem **199**:110758.

46. **Navarro M**, **Betancourt A**, **Hernández C**, **Marchán E**. 2008. Palladium Polypyridyl Complexes: Synthesis, Characterization, DNA Interaction and Biological Activity on Leishmania (L.) mexicana. J Braz Chem Soc **19**:1355–1360.

47. **Serrano FA**, **Matsuo AL**, **Monteforte PT**, **Bechara A**, **Smaili SS**, **Santana DP**, **Rodrigues T**, **Pereira F V**, **Silva LS**, **Machado Jr J**, **Santos EL**, **Pesquero JB**, **Martins RM**, **Travassos LR**, **Caires ACF**, **Rodrigues EG**. 2011. A cyclopalladated complex interacts with mitochondrial membrane thiol-groups and induces the apoptotic intrinsic pathway in murine and cisplatin-resistant human tumor cells. BMC Cancer **11**:1–16.

48. **Mutlu O**. 2014. In Silico Molecular Modeling and Docking Studies on the Leishmanial Tryparedoxin Peroxidase. Brazilian Arch Biol Technol An Int J **57**:244–252.

49. **Corral MJ**, **Benito-Peña E**, **Jiménez-Antón MD**, **Cuevas L**, **Moreno-Bondi MC**, **Alunda JM**. 2016. Allicin Induces Calcium and Mitochondrial Dysregulation Causing Necrotic Death in Leishmania. PLoS Negl Trop Dis **10**:e0004525.

50. **Docampo R**, **Vercesi AE**, **Huang G**. 2014. Mitochondrial calcium transport in Trypanosomes. Mol Biochem Parasitol **196**:108–116.

51. **Sen N**, **Das BB**, **Ganguly A**, **Mukherjee T**, **Bandyopadhyay S**, **Majumder HK**. 2004. Camptothecin-induced imbalance in intracellular cation homeostasis regulates programmed cell death in unicellular hemoflagellate Leishmania donovani. J Biol Chem **279**:52366–52375.

52. **Kowaltowski AJ**, **Castilho RF**, **Vercesi AE**. 2001. Mitochondrial permeability transition and oxidative stress. FEBS Lett **495**:12–15.

53. **Marchi B**, **Burlando B**, **Panfoli I**, **Viarengo A**. 2000. Interference of heavy metal cations with fluorescent Ca2+ probes does not affect Ca2+ measurements in living cells. Cell Calcium **28**:225–231.

54. **Takahashi A**, **Camacho P**, **Lechleiter JD**, **Herman B**. 1999. Measurement of Intracellular Calcium. Physiol Rev **79**:1089–1125.

55. **Docampo R**, **Scott DA**, **Vercesi AE**, **Moreno SNJ**. 1995. Intracellular Ca2+ storage in acidocalcisomes of Trypanosoma cruzi. Biochem J **310**:1005–1012.

56. **Moncoq K**, **Trieber CA**, **Young HS**. 2007. The Molecular Basis for Cyclopiazonic Acid Inhibition of the Sarcoplasmic Reticulum Calcium Pump. J Biol Chem **282**:9748–9757.

57. **Linares IAP**, **de Oliveira KT**, **Perussi JR**. 2017. Chlorin derivatives sterically-prevented from self-aggregation with high antitumor activity for photodynamic therapy. Dye Pigment **145**:518–527.

58. **Zuma AA**, **Mendes IC**, **Reignault LC**, **Elias MC**, **de Souza W**, **Machado CR**, **Motta MCM**. 2014. How Trypanosoma cruzi handles cell cycle arrest promoted by camptothecin, a topoisomerase I inhibitor. Mol Biochem Parasitol **193**:93–100.

59. **Prada CF**, **Álvarez-Velilla R**, **Balaña-Fouce R**, **Prieto C**, **Calvo-Álvarez E**, **Escudero-Martínez JM**, **Requena JM**, **Ordóñez C**, **Desideri A**, **Pérez-Pertejo Y**, **Reguera RM**. 2013. Gimatecan and other camptothecin derivatives poison Leishmania DNA-topoisomerase IB leading to a strong leishmanicidal effect. Biochem Pharmacol **85**:1433–1440.

60. **Reguera RM**, **Díaz-González R**, **Pérez-Pertejo Y**, **Balaña-Fouce R**. 2008. Characterizing the bi-subunit type IB DNA topoisomerase of Leishmania parasites; a novel scenario for drug intervention in trypanosomatids. Curr Drug Targets **9**:966–78.

61. **Figarella K**, **Uzcategui NL**, **Beck A**, **Schoenfeld C**, **Kubata BK**, **Lang F**, **Duszenko M**. 2006. Prostaglandin induced programmed cell death in Trypanosoma brucei involves oxidative stress. Cell Death Differ **13**:1802–1814.

62. **Edinger AL**, **Thompson CB**. 2004. Death by design: Apoptosis, necrosis and autophagy. Curr Opin Cell Biol **16**:663–669.

63. **Santana DP**, **Faria PA**, **Paredes-Gamero EJ**, **Caires ACF**, **Nantes IL**, **Rodrigues T**. 2009. Palladacycles catalyse the oxidation of criticals thiols of the mitochondrial membrane proteins and lead to mitochondrial permeabilization and cytocrome c release associated with apoptosis. Biochem J **417**:247–256.

64. **Vincent IM**, **Racine G**, **Légaré D**, **Ouellette M**. 2015. Mitochondrial Proteomics of Antimony and Miltefosine Resistant Leishmania infantum. Proteomes **3**:328–346.

65. **Mishra J**, **Singh S**. 2013. Miltefosine resistance in Leishmania donovani involves suppression of oxidative stress-induced programmed cell death. Exp Parasitol **135**:397–406.

66. **Canuto GAB**, **Castilho-Martins EA**, **Tavarez MFM**, **Rivas L**, **Barbas C**, **López-Gonzálvez Á**. 2014. Multi-analytical platform metabolomic approach to study miltefosine mechanism of action and resistance in Leishmania. Anal Bioanal Chem **406**:3459–3476.

67. **Müller S**, **Liebau E**, **Walter RD**, **Krauth-Siegel RL**. 2003. Thiol-based redox

metabolism of protozoan parasites. Trends Parasitol **19**:320–328.

68. **Krauth-siegel RL**, **Comini MA**. 2008. Redox control in trypanosomatids , parasitic protozoa with trypanothione-based thiol metabolism. Biochim Biophys Acta **1780**:1236–1248.

69. **Turrens JF**. 2004. Oxidative stress and antioxidant defenses: a target for the treatment of diseases caused by parasitic protozoa. Mol Aspects Med **25**:211–220.

70. **Barr SD**, **Gedamu L**. 2003. Role of peroxidoxins in Leishmania chagasi survival. Evidence of an enzymatic defense against nitrosative stress. J Biol Chem **278**:10816–10823.

71. **Harder S**, **Bente M**, **Isermann K**, **Bruchhaus I**. 2006. Expression of a mitochondrial peroxiredoxin prevents programmed cell death in Leishmania donovani. Eukaryot Cell **5**:861–870.

72. **Lemasters JJ**, **Nieminen A-L**. 2002. Mitochondrial Implication in Cell DeathMitochondria in pathogenesis. Kluwer Academic Publishers, New York, Boston, Dordrecht, London, Moscow.

73. **Docampo R**, **Huang G**. 2015. Calcium signaling in trypanosomatid parasites. Cell Calcium **57**:194–202.

74. **Stefani D De**, **Rizzuto R**. 2014. Molecular control of mitochondrial calcium uptake. Biochem Biophys Res Commun **449**:373–376.

75. **Scarpelli PH**, **Pecenin MF**, **Garcia CRS**. 2021. Intracellular Ca2+ Signaling in Protozoan Parasites: An Overview with a Focus on Mitochondria. Int J Mol Sci **22**:469.

76. **Baksh S**, **Burns K**, **Andrin C**, **Michalak M**. 1995. Interaction of calreticulin with protein disulfide isomerase. J Biol Chem **270**:31338–31344.

77. **Groenendyk J**, **Lynch J**, **Michalak M**. 2004. Calreticulin, Ca2+, and calcineurin - signaling from the endoplasmic reticulum. Mol Cells **17**:383–389.

78. **Lim S**, **Chang W**, **Lee BK**, **Song H**, **Hong JH**, **Lee S**, **Song B-W**, **Kim H-J**, **Cha M-J**, **Jang Y**, **Chung N**, **Choi S-Y**, **Hwang K-C**. 2008. Enhanced calreticulin expression promotes calcium-dependent apoptosis in postnatal cardiomyocytes. Mol Cells **25**:390–396.

79. **Dolai S**, **Adak S**. 2014. Endoplasmic reticulum stress responses in Leishmania. Mol Biochem Parasitol **197**:1–8.

80. **Mayer M**, **Kies U**, **Kammermeier R**, **Buchner J**. 2000. BiP and PDI cooperate in the oxidative folding of antibodies in vitro. J Biol Chem **275**:29421–29425.

81. **Kaczanowski S**, **Sajid M**, **Reece SE**. 2011. Evolution of apoptosis-like programmed cell death in unicellular protozoan parasites. Parasit Vectors **4**:44.

82. **Lemasters JJ**, **Nieminen A-L**, **Qian T**, **Trost LC**, **Elmore SP**, **Nishimura Y**, **Crowe RA**, **Cascio WE**, **Bradham CA**, **Brenner DA**, **Herman B**. 1998. The mitochondrial permeability transition in cell death: a common mechanism in necrosis, apoptosis and autophagy. Biochim Biophys Acta **1366**:177–196.

83. **Kim J-S**, **He L**, **Lemasters JJ**. 2003. Mitochondrial permeability transition: A common pathway to necrosis and apoptosis. Biochem Biophys Res Commun **304**:463–470.

84. **Lemasters JJ**, **Theruvath TP**, **Zhong Z**, **Nieminen A-L**. 2009. Mitochondrial Calcium and the Permeability Transition in Cell Death. Biochim Biophys Acta **1787**:1395–1401.

1051 85. **Tagliarino C**, **Pink JJ**, **Dubyak GR**, **Nieminen A-L**, **Boothman DA**. 2001.
1052 Calcium is a key signaling molecule in beta-lapachone-mediated cell death. J
1053 Biol Chem **276**:19150–19159.

1054 86. **de Almeida ET**, **Mauro AE**, **Santana AM**, **Ananias SR**, **Godoy Netto A V.**,
1055 **Ferreira JG**, **Santos RHA**. 2007. Self-assembly of organometallic Pd(II)
1056 complexes via CH3···π interactions: the first example of a cyclopalladated
1057 compound with herringbone stacking pattern. Inorg Chem Commun **10**:1394–
1058 1398.

1059 87. **Silva LHP**, **Nussenzweig V**. 1953. Sobre uma cepa de Trypanosoma cruzi
1060 altamente virulenta para o camundongo branco. Folia Clin Biol **20**:191–208.

1061 88. **de Almeida L**, **Passalacqua TG**, **Dutra LA**, **da Fonseca JNV**, **Nascimento**
1062 **RFQ**, **Imamura KB**, **de Andrade CR**, **dos Santos JL**, **Graminha MAS**. 2017.
1063 In vivo antileishmanial activity and histopathological evaluation in Leishmania
1064 infantum infected hamsters after treatment with a furoxan derivative. Biomed
1065 Pharmacother **95**:536–547.

1066 89. **Lima HC**, **Bleyenberg JA**, **Titus RG**. 1997. A simple method for quantifying
1067 Leishmania in tissues of infected animals. Parasitol Today **13**:80–82.

1068 90. **GÖRG A**. 2004. 2-D electrophoresis: principles and methods. Munich.

1069 91. **Tschoeke DA**, **Nunes GL**, **Jardim R**, **Lima J**, **Dumaresq ASR**, **Gomes MR**,
1070 **Pereira LDM**, **Loureiro DR**, **Stoco PH**, **Leonel H**, **Guedes DM**, **Miranda AB**
1071 **De**, **Pitaluga A**, **Jr FPS**, **Probst CM**, **Dickens NJ**, **Mottram JC**, **Grisard EC**,
1072 **Dávila AMR**. 2014. The Comparative Genomics and Phylogenomics of
1073 Leishmania amazonensis Parasite. Evol Bioinforma **8**:131–153.

1074 92. **Fonseca-Silva F**, **Inacio JDF**, **Canto-Cavalheiro MM**, **Almeida-Amaral EE**.

2011. Reactive oxygen species production and mitochondrial dysfunction contribute to quercetin induced death in Leishmania amazonensis. PLoS One **6**:e14666.

93. **Mukherjee P**, **Majee SB**, **Ghosh S**, **Hazra B**. 2009. Apoptosis-like death in Leishmania donovani promastigotes induced by diospyrin and its ethanolamine derivative. Int J Antimicrob Agents **34**:596–601.

TABLE 1 Antileishmanial activity of **CP2** against *Leishmania infantum* (IC_{50}). Data are the mean and standard deviation from three independent experiments. The results are expressed in (μmol L^{-1}).

	L. infantum IC_{50} ± SD (SI)*	
Compound	**Promastigote**	**Amastigote**
CP2	4.0 ± 0.4 (126.1)	4.7 ± 0.1 (107.6)
AmpB	0.9 ± 0.1 (25.1)	2.9 ± 0.1 (7.7)

*The selectivity index (SI, indicated in parentheses) was calculated as the CC_{50}/IC_{50} of **CP2**. $p < 0.05$ for all values.